Available online at www.sciencedirect.com
SCIENCE DIRECT®
Earth-Science Reviews 65 (2004) 195–222
EARTH-SCIENCE REVIEWS
www.elsevier.com/locate/earscirev

Reverse migration of seismicity on thrusts and normal faults

E. Carminati[a,*], C. Doglioni[a], S. Barba[b]

[a] Dipartimento di Scienze della Terra, Università La Sapienza, P.le A. Moro 5, Box 11, 00185 Rome, Italy
[b] Istituto Nazionale di Geofisica e Vulcanologia, Via di Vigna Murata, 605, I-00143 Rome, Italy

Received 30 October 2002; accepted 4 June 2003

Abstract

In this work, the control exerted by the stress axes orientation on the evolution of seismic sequences developing in compressive and extensional regimes is analysed. According to the Anderson fault theory, the vertical stress is the minimum principal stress in compressional tectonic regimes, whereas it is the maximum principal stress in extensional regimes. Using Mohr diagrams and discussing the present knowledge about the distribution of vertical and horizontal stress with depth we show that, in absence of localised fluid overpressure, such changes imply that thrust and normal faults become more unstable at shallower and greater depths, respectively. These opposite mechanical behaviours predict, in a rather isotropic body, easier rupture at shallower level in compressional regimes later propagating downward. On the contrary, a first deep rupture propagating upward is expected in extensional regimes. This is consistent with observations from major earthquakes from different areas in the world. We show that the exceptions to downward migration along thrusts occur along steeply inclined faults and probably imply localised supra-hydrostatic fluid pressures. Moreover, we show that the inversion of the meaning of the lithostatic load has consequences also for the role of topography. High topography, increasing the vertical load, should inhibit earthquake development in compressional environments and should favour it in extensional settings. Although several factors, such as geodynamic processes, local tectonic features and rock rheology, are likely to control earthquake locations, stress distribution and tectonic regime, these model predictions are consistent with seismicity distribution in Italy, central Andes and Himalaya. In these areas, large to medium compressional earthquakes occur at the low elevation borders of compressional mountain belts, whereas large extensional earthquakes occur in correspondence to maximum elevations.

Keywords: Seismicity migration; Thrusts; Normal faults; Aftershocks; Earthquakes; Crustal stress

1. Introduction

Aftershocks are interpreted as the response to stress variations induced by mainshock-related slip along active faults. It has been observed that early aftershocks coincide, for simple fault geometry, with the fault plane and are therefore related to slip along the plane itself, whereas late aftershocks are distributed in wider areas, not necessarily coinciding with the main fault plane and are considered to better define the total dimension of the fractured rock volume (Richins et al., 1987; Dietz and Ellsworth, 1990). In complex areas, where deformation is partitioned on more than one fault, recognition of main structures by early aftershocks is not straightforward. Off-fault aftershock

* Corresponding author.
E-mail addresses: eugenio.carminati@uniroma1.it (E. Carminati), carlo.doglioni@uniroma1.it (C. Doglioni), barba@ingv.it (S. Barba).

0012-8252/03/$ - see front matter © 2004 Elsevier B.V. All rights reserved.
doi:10.1016/S0012-8252(03)00083-7

clusters have been often related to static stress increases after a mainshock (Das and Scholz, 1981; Harris, 1998). On the other hand, in-fault seismicity has been related to the presence, and subsequent rupture, of asperities (Aki, 1992). This work deals with in-fault seismicity migration in the dip direction on thrust and normal faults occurring at shallow-intermediate crustal levels (approximately 0–20 km), giving insights in the physics of earthquakes.

Although it is widely accepted that the nucleation of large-intermediate earthquakes occur preferentially at the base of the seismogenic layer (Sibson, 1982, 1983; Das and Scholz, 1983), at least one deviation from this 'rule' has been previously reported (Vogfjörd and Langston, 1987). In this work, we show that a significant number of compressional earthquakes nucleated at shallow depth and showed downward propagation of seismicity. Our observations integrate those dealt within Sibson (1982), showing a seismic behaviour more complex than generally accepted. The knowledge that compressional seismicity can propagate downward can influence both the seismic hazard assessment and how we can deal with a possible foreshock.

In the following, earthquake sequences are reviewed from several areas in the world. It is shown that, in a significantly large number of cases in compressional regimes, fractures preferentially generate at shallow depths and propagate downward, while the opposite occurs in extensional regimes (Doglioni, 2000). We later review borehole stress measurements and discuss commonly accepted ideas on the distribution of horizontal and vertical stresses with depth. Then we propose and discuss a possible explanation of the observed reverse migration of seismicity, on the basis of Anderson's faulting theory (Anderson, 1951), and evaluate its consequences. We finally discuss the role of topography in extensional and compressional regimes.

2. A selection of earthquakes occurred world-wide

A large selection of earthquakes occurred world-wide was made in order to verify if upward and downward migration of seismicity can be assessed in a wide data set. Since upward migration is commonly accepted in extensional tectonic regimes, for sake of brevity we will focus mainly on compressive regimes, where a different behaviour has been evidenced (Vogfjörd and Langston, 1987).

Most known compressional earthquakes are also the strongest ones and are related to under-thrust of lithosphere in collisional regimes. Many of them occur at large depths, usually greater than 15–20 km. In this work, we deal with the 0–20 km depth range, where tectonic and stress features are better constrained. Therefore we will consider mainly earthquakes due to shallow thrusting in the outermost portions of fold and thrust belts. In these cases, magnitude of mainshocks can be as low as 5.0, or even lower. In the case of very thin thrust sheets, earthquakes can also be not accurately locatable if the seismic network is sparse. Lower magnitude events are usually less studied; as a consequence good quality data are not widespread.

To analyse seismicity migration before and after the occurrence of a mainshock, we used high resolution data. Such data are usually available where permanent seismic networks are very dense, where a detailed velocity model is available, and when temporary seismic networks are deployed. Often, foreshocks and early aftershocks data have inadequate resolution. Accuracy is generally better for the aftershock locations since surveys are deployed after the mainshock occurs. We decided not to perform an automatic selection of data among available catalogues, as performing an error analysis on the whole data set could introduce further complications in this study. Besides, we aim at reducing the risk of mistakes due to the inaccurate earthquake locations or insufficient knowledge of upper-crustal structure. For these reasons, we handpicked interesting cases in compressive environments, where: (i) a dense seismic network is operating in the area of the earthquake; (ii) tectonic features are well known by surface geology and deep seismic sections; (iii) a detailed seismic velocity model is available in the earthquake area; and (iv) the earthquake location method is well described in literature. This selection does not ensure completeness but allows conclusions to be drawn in well-known areas. We also include some Californian earthquakes, although they show a significant strike slip component.

We discuss the normal-faulting earthquakes of 1980, Ms 6.9 Irpinia (Italy); 1983, Ms 7.3 Borah Peak (Idaho, US); 1997, Mw 6.0 Colfiorito (Italy), and the reverse-faulting earthquakes of 1968, Ms 6.8 Mecker-

ing (Australia); 1976, Ml 6.4 Friuli (Italy); 1977, Ms 7.4 Caucete (Argentina); 1985, Ms 6.9 Nahanni (Canada); 1988, Ms 6.7 Tennant Creek (Australia); 1989, Ms 6.9 Spitak (Armenia); 1989, Ms 6.9 Loma Prieta (California, US); 1991, Ms 7.0 Racha–Dzhava (Georgia, CIS); 1994, Ms 6.7 Northridge (California, US); 1997, Ml 4.6 Strait of Georgia (Canada); 2000, Ml 4.5 Faenza (Italy). All these compressional earthquakes show downward migration of seismicity. Then, we discuss some exceptions. The description of the sampled earthquake sequences follows.

2.1. Earthquakes in extensional tectonics

2.1.1. The 1980 Irpinia, Italy, earthquake

Italy is characterised by extensional tectonics in the hanging-wall of the W-directed subduction of Adriatic lithosphere which is generally related to back-arc extension induced by the eastward to southeastward retreat of the subducting slab (Scandone, 1980; Malinverno and Ryan, 1986). The 1980 Irpinia and the 1997 Colfiorito earthquakes developed within this scenario.

The Irpinia 23 November 1980 earthquake (Fig. 1) in the Southern Apennines was generated by two normal faults dipping northeastward and one conjugate, with Ms 6.9 (Bernard and Zollo, 1989). The earthquake showed the largest moment release at a depth of 8–13 km (Giardini, 1996) and a possible nucleation at about 10 km. Most of the aftershocks were generated in the hanging wall of the main fault, between this and an antithetic normal fault dipping to the southwest (Amato and Selvaggi, 1993). All the aftershocks occurred at depths (3–10 km) shallower than the mainshock (Amato and Selvaggi, 1993).

2.1.2. The 1983 Borah Peak, ID, earthquake

The October 28, 1983 Borah Peak earthquake (Ms = 7.3) is the largest ever recorded in Idaho, in a area with low historical seismicity. It produced a 34-km-long zone of scarps and ground breakage, trending northwest and located along the southwest slope of the Lost River Range. The visible slip along the fault trace ranged up to 2.7 m at the base of Borah Peak (Wallace, 1984; Chrone et al., 1987). A regional network was operating when the mainshock occurred, which did not record foreshock with coda magnitude Mc>2.0 in the previous 2 months, and no earthquakes with M>3.5 were reported for at least 20 years prior to the mainshock (Dewey, 1984). Both surface fractures and the short period focal mechanism (Doser and Smith, 1995) indicate that the motion occurred along a normal fault. A dense, portable seismograph network, with 2 to 10 km of station spacing was deployed a few hours after the mainshock, and recorded almost 400 locatable aftershocks. The availability of refraction profiles in the vicinity provided information on the velocity structure (Sparlin et al., 1982), thus allowing accurate aftershocks location. By means of a master-event technique, the mainshock was relocated at a depth of 14 km ca. southeast of the surface faulting (Richins et al., 1987). The results showed an upward, unilateral rupture propagating northwestward, and this result satisfactorily accounts for the aftershock occurrence.

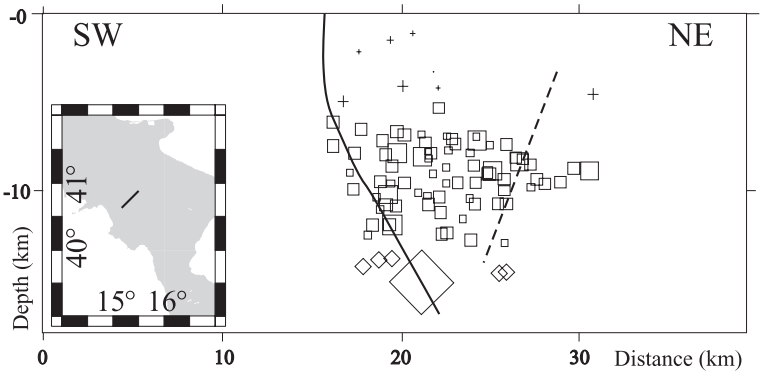

Fig. 1. Cross-section of the Irpinia 1980 normal fault-related earthquake sequence. The largest square is the mainshock. It can be noted that the aftershocks are shallower. Modified after Amato and Selvaggi (1993).

2.1.3. The 1997 Colfiorito, Italy, earthquake

The Colfiorito extensional basin in the Central Apennines lies in the extensional band also studied by Frepoli and Amato (1997). In this area, a seismic swarm began on September 3, 1997 with a Mw = 4.5 earthquake. On September 26, 1997 two major earthquakes (Mw = 5.7 and Mw = 6.0, respectively) occurred near the village of Colfiorito (Fig. 2) and ruptured two adjacent segments of the same fault. Both mainshocks CMT solutions of the two events indicate extensional motion (Olivieri and Ekstroem, 1999). Fault plane solutions derived by analysing near-source strong-motion recordings (Zollo et al., 1999) are projected on the vertical section of Fig. 2b. Rupture occurred along two adjacent segments of the same fault during the two events. Teleseismic observations have shown that the slip and centroid of these two events were shallower than hypocentre depth, implying an upward directivity of the source

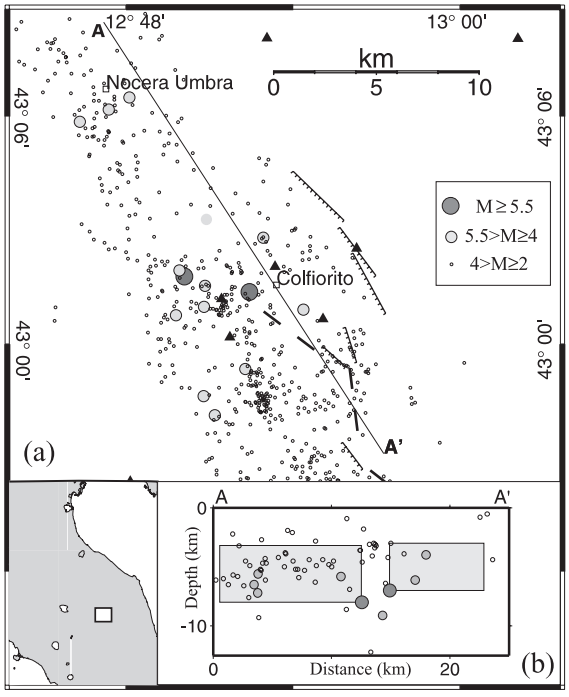

Fig. 2. Map (a) and strike cross-section (b) showing the early aftershocks (occurred between September 26 and October 3, 1997) of the Umbria 1997 normal fault earthquake swarm located by Barba and Basili (2000). The grey boxes indicate activated fault planes (after Zollo et al., 1999). As in Fig. 1, aftershocks are shallower than the mainshock.

(Zollo et al., 1999). Early aftershocks (occurred between September 26 and October 3, 1997), relocated by Barba and Basili (2000), are shown in the map of Fig. 2a and in the section of Fig. 2b. Given the maximum errors of 1.1 km on hypocentral depth it can be observed that early aftershocks reasonably coincide with the area of mainshock fault planes confirming the estimated subsurface dimension of the faults. It can also be observed that practically all of the aftershocks occurred at depths shallower than the two mainshocks, whilst the September 3 foreshock occurred at greater depth.

2.2. Earthquakes in compressional tectonics

In this section, we describe compressional earthquakes characterised by downward migration of seismicity. We favour purely compressional cases, i.e., earthquakes occurring in fold and thrust belts and intraplate events. For completeness, however, we include some Californian earthquakes, although they develop in a transpressive tectonic setting.

2.2.1. The 1968 Meckering, Australia, earthquake

The October 14, 1968, Ms 6.8 Meckering earthquake was located in the SW corner of the Australian continent, in an area of relatively flat topography and was one of the biggest earthquakes of the continent. It produced a North trending fault scarp more than 32 km long (Everingham et al., 1969) and surface breakage for over 200 km. At the surface, the average slip was about 2 m, with a maximum observed slip of 3.5 m. Aftershocks lasted for many months, affecting distances up to 80 km.

The fault plane solution of the mainshock indicates almost pure reverse faulting, with N–S strike. According to surface observations, the fault plane is the E-dipping one, and body waveform inversion indicates a dip possibly ranging from 31 to 37 (Vogfjörd and Langston, 1987; Fredrich et al., 1988). The centroid depth results to be about 3 km (Fredrich et al., 1988), and this value appears to be well constrained by the amplitude of P- and SH-waves. The very shallow centroid is also confirmed by the fault scarp well evident in the field, which exhibited ~ 2 m of coseismic uplift (Everingham et al., 1969), a maximum slip of 3.5 m and an average slip on the fault plane of ~ 0.75 m (Fredrich et al., 1988). These information

can be consistent if we consider the slip decreasing from the top of the fault to the bottom.

Vogfjörd and Langston (1987) also modelled the fracture propagation with given velocity along a finite fault by means of trial-and-error approach. Among the possible models, they tested down-dip and up-dip fracture propagation along the thrust plane. The best fit was reached with a fracture starting at 1 km depth and propagating downward. Although a simplified model of the fault was used, the fit was surprisingly good also on short period waveforms.

Even if no data can actually constrain the depth of rupture nucleation for the Meckering earthquake, both coseismic and short period data strongly suggest a focus that is close to the surface, and a rupture which propagates downward and stops at depth of nearly 6 km.

2.2.2. The 1976 Friuli, Italy, earthquake

The 1976 Friuli earthquakes (Fig. 3) generated in two main episodes, May 6 and September 15, with magnitudes 6.4 and 6.1, respectively. The focal mechanisms are mainly compressional, with a slight transpressional component (Slejko et al., 1999). They were associated with N-dipping thrust planes in the eastern part of the Southern Alps, at the intersection with the Dinarides thrust belt in northeast Italy. The maximum energy released by the aftershocks of the May 6 earthquake was very shallow, between 2 and 8 km. The highest energy release density has been evaluated to be located at a depth of about 4 km (Amato et al., 1976). The epicentres of the later September quakes and related aftershocks were about 8 km northward. These September hypocentres were deeper (down to 16–17 km) and characterised by a maximum energy release density at about 5–6 km (Amato et al., 1976).

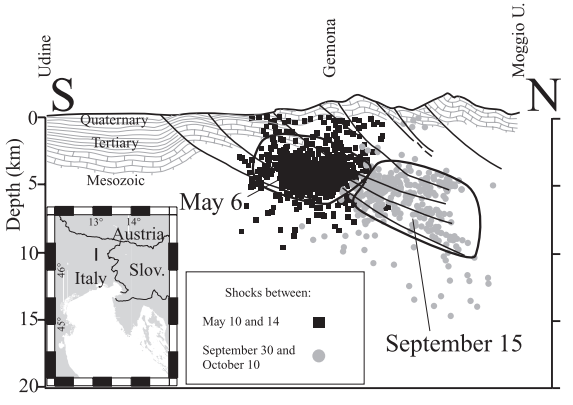

Fig. 3. Cross-section of the Friuli 1976 earthquake sequences occurred in a compressive environment. Modified after Amato et al. (1976). The timing of groups of events clearly show a deepening of seismic activity with time.

During 3 years preceding the 1976 Friuli earthquakes, a continuous southward ground tilt was recorded by a underground tiltmeter placed near a neighbouring secondary fault 15 km northwest of the epicentre of the impending earthquake (Braitenberg and Zadro, 1999). The cumulative ground tilt amounted to as much as 3 min of arc (Biagi et al., 1976) and has been modelled by Dragoni et al. (1985) as due to aseismic slip occurring on the shallowest portion (less than 1 km) of the near secondary fault. Such fault belongs to the same fault system of the seismogenic source of the 1976 earthquakes and therefore is supposed to be affected by the same stress accumulation mechanism. The sequence of the stress release is hence schematised in: (i) aseismic slip on the shallowest portion (less than 1 km) during 3 years (1973–1976); (ii) May 1976, occurrence of the Ms 6.4 earthquake and its aftershock sequence (2–8 km); (iii) September 1976, occurrence of the Ms 6.1 earthquake and its aftershock sequence (down to 16–17 km). These data strongly constrain the downward propagation of both seismicity and related phenomena. This feature seems to be recurrent, as the relationship between the aseismic tilt and the regular earthquakes occurred at least once earlier, in 1954 (Caloi and Spadea, 1955).

2.2.3. The 1977 Caucete, Argentina, earthquake

The November 23, 1977, Ms 7.4 Caucete earthquake occurred in the Sierras Pampeanas, in western Argentina (Fig. 4). This tectonic province overly the region where the Nazca plate subducts nearly horizontally beneath the South America plate. Neotectonic features are due to a nearly EW oriented compression in the area.

The mainshock occurred at a depth of 17 ± 5 km (Chinn and Isacks, 1983), and was preceded by a foreshock which occurred at the same depth. The foreshock and mainshock occurred respectively close to the northern and southern ends of the aftershock zone (Kadinsky-Cade et al., 1985) The CMT shows a

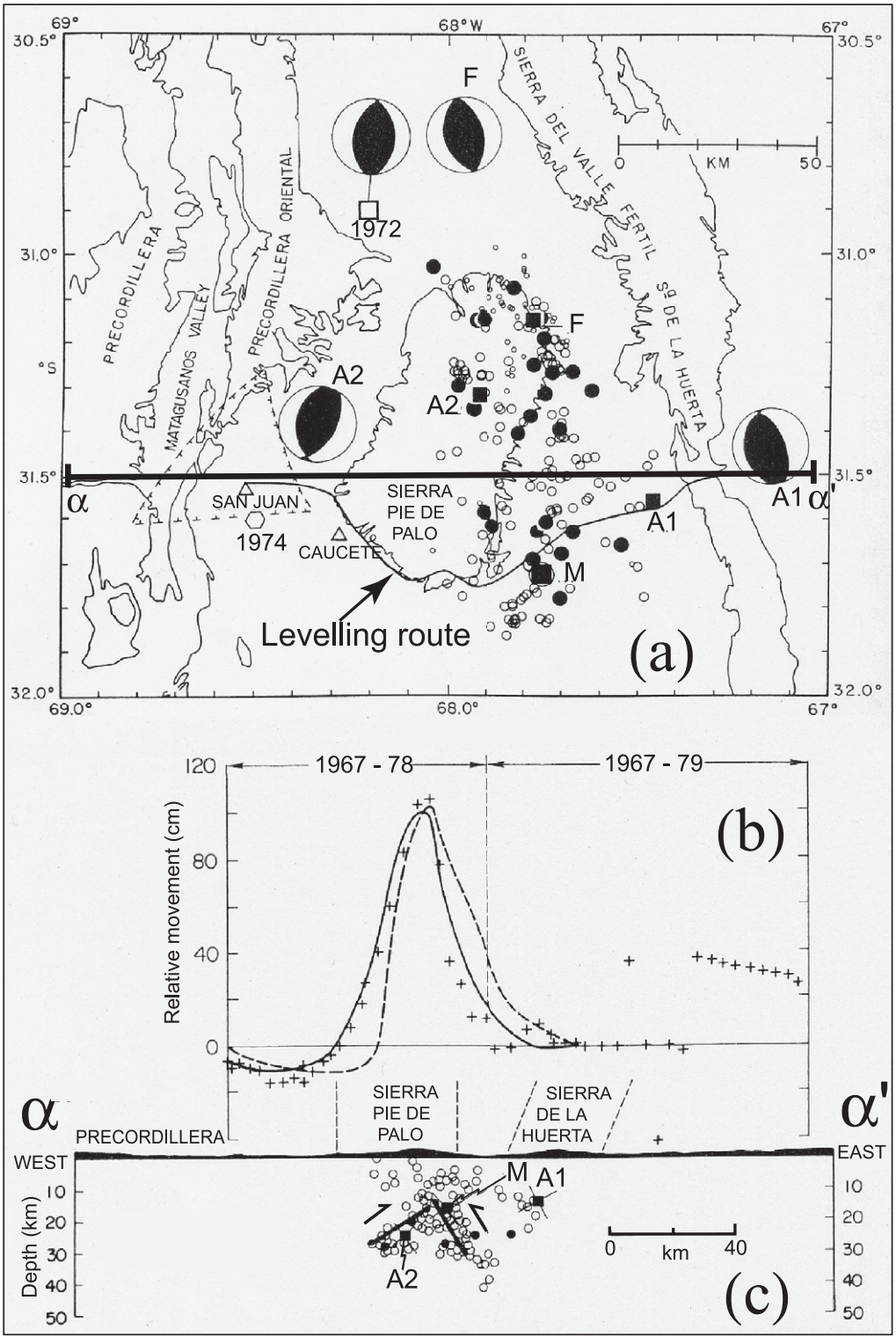
69°
68°W
67°
30.5°
31.0°
31.5°
32.0°
°S
69.0°
68.0°
67°
F
1972
A2
A1
α
α'
M
0 KM 50
SIERRA DEL VALLE FERTIL
Sa DE LA HUERTA
PRECORDILLERA
MATAGUSANOS VALLEY
PRECORDILLERA ORIENTAL
SAN JUAN
1974
CAUCETE
SIERRA PIE DE PALO
Levelling route
(a)
120
80
40
0
1967 - 78
1967 - 79
Relative movement (cm)
(b)
SIERRA PIE DE PALO
SIERRA DE LA HUERTA
PRECORDILLERA
WEST
EAST
Depth (km)
10
20
30
40
50
0 km 40
(c)

nearly pure reverse mechanism, consistent with the known stress state of the area, with centroid depth at about 21 km. Coseismic uplift was about 1.2 m, and observed surface faulting was interpreted as a secondary effect of the uplift of the range.

A seismic survey was carried out by USGS after the mainshock and lasted for 11 days. Aftershocks recorded during this time have been discussed (Kadinsky-Cade et al., 1985 and references therein). The shallow velocity model was constrained by available refraction data. Aftershocks occurred in the following 4 months were recorded by teleseismic stations and located using a master event/common station technique. The aftershocks formed two groups that dip both east and west, although simple planes could not be defined.

Levelling data allowed to constrain the fault plane of the mainshock (Fig. 4). Kadinsky-Cade et al. (1985) showed that two main features in the coseismic uplift profile were crucial to identify the fault plane of the mainshock. First of all, they observed that the maximum coseismic uplift did not coincide with the maximum of topography. As a consequence, they assessed 2 cm as an upper limit of topography-related errors on the levelling measurements. Then, the asymmetry of the observed uplift (steeper tilting on the east side, little subsidence on the west side) clearly favoured the west dipping model. By means of trial-and-error procedure, Kadinsky-Cade et al. (1985) assigned a fault dipping 35 to the west, with down-dip length of 24 km. 4 m of slip was required to fit the observed uplift. The west-dipping model is also supported by the position of the largest aftershocks, which lie to the west. A small steepening is required the top of the mainshock fault, in order to match a small wavelength feature in the observed uplift pattern. The authors conclude that the rupture initiated near the top end of the fault and propagated downward. Both the coseismic model, the mainshock and centroid depths, and aftershock locations are consistent with this conclusion.

2.2.4. The 1985 Nahanni, Canada, earthquakes

Two large magnitude earthquakes occurred in October 5, 1995 (Ms 6.5), and December 23, 1995 (Ms 6.9) in the Canadian eastern Cordillera. The area is subjected to horizontal compressive stress oriented NE–SW and exhibits thrust faults striking southeast. The terrain was generally low relief and no evidence of surface breaks were detected after either earthquake. In the area, already surveyed by the Canadian seismograph network, three accelerographs (Weichert et al., 1986) and 5 to 7 seismometers (Wetmiller et al., 1988) were deployed after the mainshock. Both earthquakes were followed by an aftershock sequence that developed for more than 60 km along the thrust strike and for about 15 km along the dip.

Both mainshocks nucleated at about 6 km, although some evidences suggested that the December event was deeper (Wetmiller et al., 1988). The second mainshock was located at no more than 3 km from the first one (Wetmiller et al., 1988) and seemed to rupture an asperity which could have acted as a barrier for the first one (Choy and Boatwright, 1988), clearly affecting a larger faulted area. The dip of the fault plane of the inverse mechanism events was low, 30–34 for the 1st mainshock and 23–25 for the 2nd (Wetmiller et al., 1988; Choy and Boatwright, 1988). The aftershocks clearly highlighted that the fault plane, among those allowed by the focal mechanisms, was the one dipping SW. The directivity of the rupture of the 2nd mainshock, according to two very close accelerographs, was SW (Weichert et al., 1986), so the fracture propagated down-dip.

Hypocentral depths and locations of the aftershocks were determined through relative locations among the Canadian and the temporary seismic networks (Wetmiller et al., 1988). The aftershocks had a depth range of 2–13 km for the first mainshock and 4–15 km for the second one (Fig. 5), with an apparent dip of 20–40 to the west. On the average, aftershocks of the second mainshock seemed to be a few kilometres deeper than for the first mainshock, and

Fig. 4. (a) Map view of aftershocks of the 1977 Caucete (Argentina) earthquake. The focal mechanisms of a few major events (A1, A2, and F) are shown. M indicates the mainshock. The curved line indicated by the arrow is the location of the levelling route of the graph of panel b. The trace of the cross section of panel c is also indicated. (b) Levelling profile indicating relative movements occurred along the route between 1967 and 1978/1979 (crosses). The results of vertical motion modelling for two scenarios (east dipping fault, dashed line and west dipping fault, solid line) is also shown. The west dipping fault scenario provides the best fit. (c) Vertical cross-section showing the location of the mainshock and aftershocks. Note that most of the aftershocks are deeper than the mainshock. The horizontal scale is the same for panels b and c which are lined up with each other. The figures are taken from Kadinsky-Cade et al. (1985).

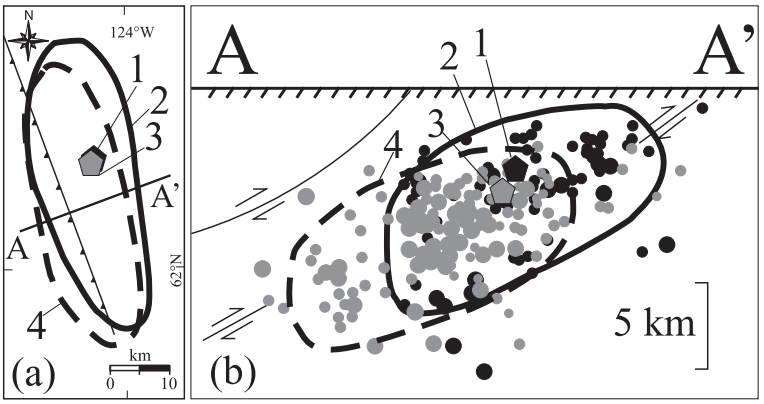

Fig. 5. Temporal distribution of seismic activity during the Nahanni 1985 earthquake in map (a) and cross-section (b) view. The full pentagon and dots represent mainshock and aftershocks of the first event, respectively (labelled 1 and 2 following their time sequence). The grey pentagon and dots represent mainshock and aftershocks of the second event, respectively (labelled 3 and 4). For a full discussion on the location of the mainshocks, please refer to the text. Redrawn and modified after Wetmiller et al. (1988).

showed a distinct westward shift. Both mainshocks ($Z \sim 6$ km) were located in the upper part of the aftershock sequence.

For these earthquakes, there is evidence of down-dip propagation of the fracture; aftershocks were mostly deeper than the mainshocks, and the second aftershock sequence was deeper than the first one (Fig. 5). Based on this last observation, it is also suggested, but not strictly required for the purpose of this paper, that the asperity of the December event was deeper than the asperity broken in October. We conclude that the Nahanni earthquakes are a clear example of down-dip propagation of seismicity.

2.2.5. The 1988 Tennant Creek, Australia, earthquakes

The Tennant Creek intraplate sequence began in a previously aseismic area with an event of magnitude Ml 5.4 on January 8, 1987 and continued for over 1 year. On January 22, 1988 three distinct, large earthquakes of magnitude Ms = 6.3, Ms = 6.5 and Ms = 6.7 occurred in less than 12 h, developing along a complex fault system in a desert area, producing a surface rupture about 35 km long, trending east–west, with the southern block overthrusting the northern one. This event produced 1 m of uplift and 2 m of horizontal displacement. Investigations have been subsequently made on the basis of teleseismic (Bowman and Dewey, 1991), local array data (Bowman, 1988) and field observations (Lettis et al., 1997, and references therein), and a local seismic network was deployed to record aftershock seismicity. The complex fault system which generated the three earthquakes is composed of three fault segments which show nearly the same east–west trace, two of which dipping mainly south and the middle one dipping north (Bowman et al., 1990). The three mainshocks exhibit a different depth with respect to the triggered aftershock volume. The Ms = 6.3 mainshock developed at a depth of 5–8 km, in correspondence of the deepest aftershock locations. On the contrary, the second Ms = 6.5 mainshock, occurred about 2 h later, was located at a depth of 3–3.5 km, in correspondence of the shallowest aftershocks. The last Ms = 6.7 mainshock occurred at a depth of 4–5 km, and was located in the middle of the corresponding aftershock sequence (all data by Choy and Bowman, 1990). We can observe that among the three mainshocks, only the first one showed an upward migration of the aftershock seismicity, while in the second and in the third case the migration has been respectively downward and symmetrical. The different focal depths and the increase in radiated energy along the three, differently dipping thrust faults can mean that, in this case, lateral variation of strength played a major role with respect to the vertical gradient of shear stress in controlling the rupture process. The Tennant Creek area may reasonably act as an isolated faulted zone in an otherwise intact crust. This hypothesis is supported also by the lack of seismicity in the region prior to 1987.

2.2.6. The 1989 Spitak, Armenia, earthquake

A destructive Ms 6.9 earthquake occurred on December 7, 1988 in Armenia (Fig. 6). The tectonics of the region is mainly driven by NS compression (Philip et al., 1989) and the faulting mechanism consisted in a thrust with a plane dipping north. Field surveys (Philip et al., 1992) and the installation of a temporary seismic network (Dorbath et al., 1992) allowed study of this earthquake.

Reverse faulting was observed at the surface. The scarp was about 8 km long, trending N120, with a maximum of 1.6 m of vertical displacement in the middle (Cisternas et al., 1989). The aftershocks followed the same trend N120, with a dip of 50, and suggested that the rupture developed in five segments (Dorbath et al., 1992), so reflecting the complexity of the source.

The central (1st) segment is the most important one and also the first to break. The associated aftershocks define a plane dipping nearly 55 north, and are bordered south by the observed scarp, and north by a major tectonic feature (Philip et al., 1992). At the southern end of the surface rupture (SE branch, 2nd segment), en-echelon surface breaks were found. The almost vertical distribution of aftershocks down to 6 km ca. and the strike slip focal mechanism of the subevent occurred across this segment; this suggests that it acted like a strike slip fault (Haessler et al., 1992). At the northern end of the surface rupture (WNW, 3rd segment), it seems that the fault is blind. Cracks alignment along the fold and aftershocks occurring down to 10 km depth indicate that this segment was activated during the earthquake. Further west, two clusters of seismicity can be identified respectively with an unbroken thrust (4th segment), which exhibits seismicity from 5 to 12 km, and with a vertical plane slightly shifted to north, with hypocentral depths ranging from 3 to 6 km depth (5th segment).

Haessler et al. (1992) constrained the source model by using the a-priori knowledge of these five segments. By means of a trial-and-error procedure, they generated synthetic seismograms, filtered the recordings of broad-band P- and SH-waves through a 5 s low-pass, and chose the source history providing the best fit among them. As a first result, they evidenced in the time-domain signals two pulses separated by about 10 s. Their duration was longer for eastern stations than for western stations, indicating westward directivity of the rupture. In fact, aftershock seismicity deepens westward and western segments rupture later.

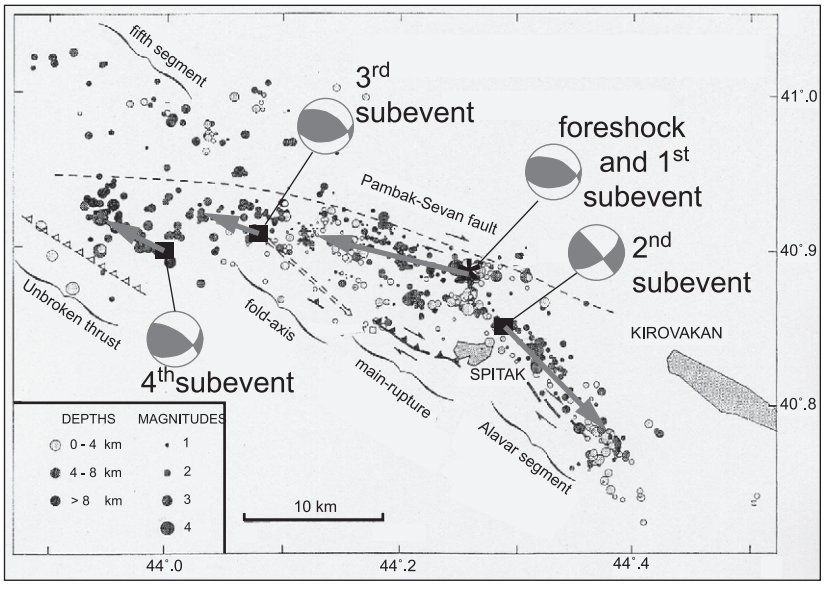

Fig. 6. Map showing the distribution of events occurred during the 1989 Spitak, Armenia earthquake. The structural setting of the area is also skematically shown. The focal mechanisms of the subevents described in the text are represented. The segments and the subevents follow the same temporal order. Modified after Haessler et al. (1992).

Reverse segments to the west (3rd, 4th) were therefore deeper than the 1th segment. These data clearly indicate that deeper segments rupture later. Haessler et al. (1992) also hypothesised the presence of a small precursor, since the first arrival was not impulsive at some stations.

Haessler et al. (1992) generated synthetics by a sequence of point sources, which extend along the aftershock zone (Dorbath et al., 1992), and divided the rupture in five segments on the basis of the above a-priori information. The rupture initiated with a small foreshock whose location was the same of the mainshock (Dorbath et al., 1992). Focusing attention on the 1st segment alone, we find a depth of the foreshock and of the first sub-event respectively of 4.5 and 5 km (Table 2 in Haessler et al., 1992), while aftershock depths ranged between 4 and 8 km. The 4th sub-event exhibits a similar behaviour, as it occurred at depth of 6 km, and was followed by aftershocks whose depth ranged between 5 and 12 km. The 3rd sub-event (localised at 6 km depth) apparently follows the same behaviour as the 1st and the 4th, but the published aftershock sections seem to be a bit too distant from the 3rd sub-event location to draw conclusions on it.

For the 1st and 4th sub-events, we conclude that aftershock as located by the temporary local network (Dorbath et al., 1992) have been deeper than the mainshock. Besides, an apparent trend of deepening of reverse fault branches with time has also been observed during the mainshock.

2.2.7. The 1991 Racha–Dzhava, Georgia, CIS, earthquake

The April 29, 1991, Ms 7.0 Racha–Dzhava earthquake occurred along a thrust fault trending east–west, dipping to north, located at the southwestern edge of the Great Caucasus. In this region, a N–S compressional regime is generated by the nearly N–S continental collision between the Arabian plate and the Russian Platform (Philip et al., 1989). Most of the active thrusts of the Caucasian region have been affected by earthquakes in the last 30 years. The earthquake developed in four episodes, and the rupture has been about 24 km long (Fuenzalida et al., 1997). Through waveform modelling, Fuenzalida et al. (1997) determined centroid parameters of the mainshock (MS) and the three sub-events (in time order, 1st sub-event, MS, 2nd and 3rd sub-events). From their Table 3, depths and dip angle of these 4 episodes are: (1st) 5.36 ± 0.4 km, 48.0 ± 1.5; (MS) 4.81 ± 0.2 km, 29.0 ± 0.6; (2nd) 10.3 ± 0.7 km, 59.7 ± 1.6; (3rd) 6.5 ± 0.6 km, 57.1 ± 3.4. It can be observed that the depths range from about 5 km for the MS and the 1st sub-event, to about 10 km for the 2nd sub-event. The sequence has been thoroughly studied by means of a dense temporary seismic network, deployed a few days after the mainshock, and broad band permanent stations. The aftershocks in the following 2 months covered an area about 80 km long and 20 km wide (Triep et al., 1995; Fuenzalida et al., 1997), leaving apparently unaffected the area already ruptured by the mainshock. Aftershocks lie along the north dipping plane, with a gentle (~ 30) angle and have depths ranging between 2 and 15 km (Fig. 7). Even if we do not want to evoke a downward propagation of the mainshock rupture, we can observe that most of the aftershock activity is deeper than the four different rupture episodes of the mainshock.

2.2.8. The 1997 strait of Georgia, British Columbia, earthquake

Among the many thrust earthquakes affecting British Columbia and Washington State, we focus our attention to a Ml = 4.6 crustal event occurred on June 24, 1997 at a depth of 3–4 km beneath the Strait of Georgia, not far from Vancouver (Fig. 8). Moderate-size, shallow earthquakes like this one or like the Ml = 5.0 earthquake felt in Vancouver in 1975 can help to assess the seismic potential of the region. They are of some interest because of the damage they can produce, although little signature can be left on the mapped near-surface faults. The Strait of Georgia has been investigated through an onshore/offshore wide-angle seismic reflection/refraction experiment (Fisher et al., 1999), as a consequence of it a 3-D velocity model for the upper crust in the area has been derived (Zelt et al., 2001). From a geological point of view, a preliminary analysis has been made by Mosher et al. (2000) to correlate the seismicity with shallow compressional structures, forming the background to a detailed seismological analysis. Cassidy et al. (2000) located the well-recorded 1997 reverse-faulting earthquake, its foreshocks and aftershocks by means of a double-difference location algorithm, by using waveform cross-correlation on a dense network. They found that the mainshock was preceded by 11 days

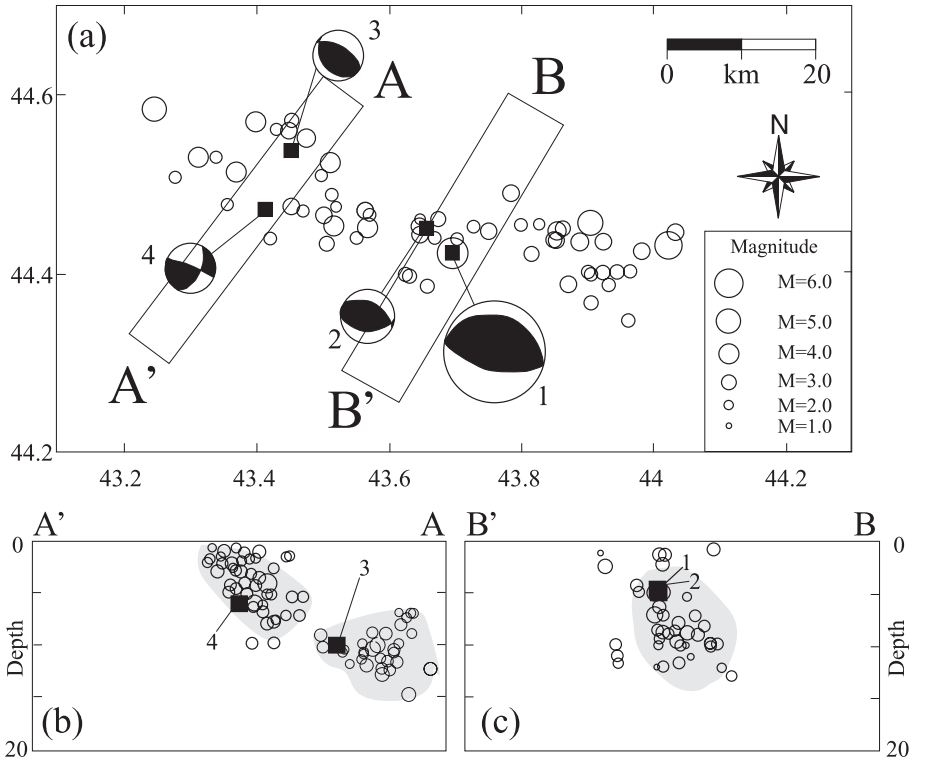

Fig. 7. Space–time distribution of seismic activity during the Racha–Dzhava 1991 earthquake. In the map (a) and in the cross-sections (b and c), the full squares represent the location of major events (labelled 1–4 following their time sequence). The circles represent the aftershocks. Redrawn and modified after Fuezalida et al. (1997).

by a Ml = 3.4 foreshock, occurred at a depth of 2 km and also felt in the area, and was followed by numerous small aftershocks, whose depth ranges down to 6 km. The temporal sequence of the relocated hypocentres exhibits an unambiguous evidence of down-dip migration of seismicity along the 47–53° dipping fault plane.

2.2.9. The 2000 Faenza, Italy, earthquake

The Faenza area in the outer part of the Northern Apennines arc, is characterised by active thrusts buried underneath the Po plain sediments. Historical events of magnitude less than Me 5.8 have been reported in the area (Boschi et al., 1997). The analysed swarm begun on April 19th, 2000 ($Z \sim 6.5$ km, evt. 2 in Fig. 9), lasted more than 1 month and has been monitored by a temporary seismic network since May, 2nd. Focal mechanisms showed to be reverse, (Calderoni et al., 2000), according with the stress state in the area. Magnitude of events increased with time, up to Ml 4.5 on May 10th ($Z \sim 18$ km, evt. 13 in Fig. 9). In order to test the hypothesis of downward migration of seismicity we analyse original data from the Istituto Nazionale di Geofisica e Vulcanologia (INGV) catalogue. To highlight a possible dependence of depth with time, we counted the number of events every 2 h and selected the largest shock in the 2-h periods which evidenced a sudden increase of the seismic activity. This procedure also evidenced a previous quake occurred on Jan, 5th, 2000 (evt. 1 in Fig. 9) that we included in the analysis.

Events shown in Fig. 9 have been localised with the INGV seismic network and show a general deepening of mainshocks with time. Hypocentral depths of earthquakes localised through the temporary network (15–20 km after May 2nd, Calderoni et al., 2000) reasonably coincide, in the period of overlap, with those found in this work, allowing us to extend the analysis to the whole swarm. For quakes later in the swarm, the lack of impulsive S

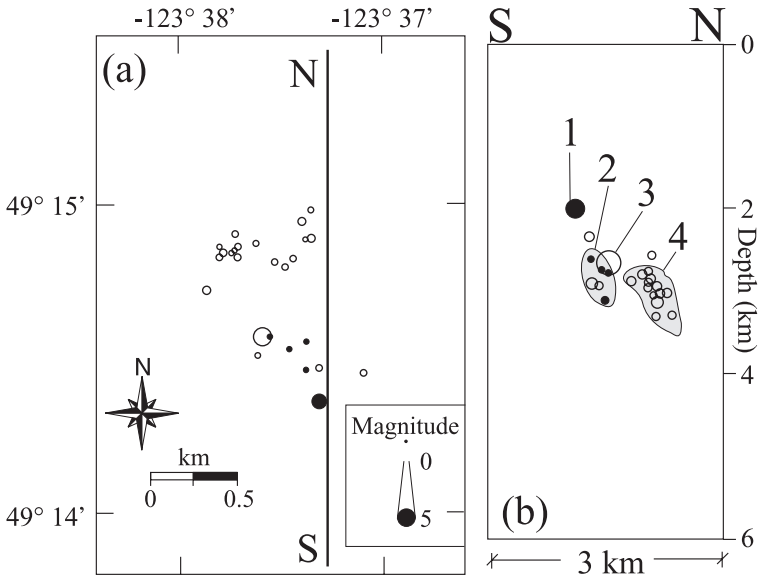

Fig. 8. Space–time distribution of seismic activity during the Strait of Georgia 1997 earthquake. In the map (panel a) and the cross-section (panel b), the full dots represent the mainshock of June 13, 1997 and its aftershocks (labelled 1 and 2, respectively, in panel b). The circles represent the mainshock of June 24, 1997 and its aftershocks occurred within the first 24 h (labelled 3 and 4, respectively, in panel b). Redrawn and modified after Cassidy et al. (2000).

wave at the closest (10 km) station and the weaker, widespread macroseismic effects reported by the population after the stronger events also support the greater depths found after May 2nd. In conclusion, in the Faenza thrust system, a significant deepening of earthquakes with time is found.

2.3. Controversial cases

Seismic activity before the mainshock is sometimes neglected. In two compressional cases, Loma Prieta and Northridge, the mainshock–aftershock sequence developed up-dip through time. However, the

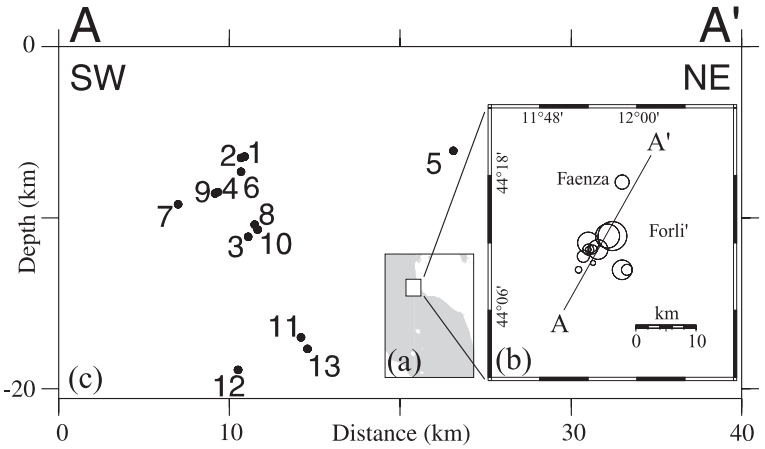

Fig. 9. Faenza 2000 compressive earthquake swarm. Panels (a) and (b) show map views. The cross-section (c) shows events associated to sudden increase of seismic activity. The event numbers increase with time, (1) 01/05/00, (2) 04/26/00,. . ., (13) 05/10/00. Note the general deepening of the events. Data from INGV.

earlier seismic activity occurs at shallower depths and shows a rough down-dip migration. Therefore, we consider these cases as controversial, suggesting a possible physical relationship between the mainshock and the earlier activity.

2.3.1. The 1989 Loma Prieta, CA, earthquake

The October 17, 1989 Loma Prieta, Mw = 6.9 earthquake occurred at a depth of 18 km (Dietz and Ellsworth, 1990) along a thrust fault with a mainly reverse focal mechanism and some strike slip component (Oppenheimer, 1990). The aftershocks were shallower and propagated up-dip along the steep (70°) fault plane of the mainshock. When considering only the mainshock–aftershock activity, this up-dip migration would contrast with what observed in the previously described cases. However, atypical seismic activity occurred in the area a few months before the mainshock. Such activity was shallower than the mainshock initiation depth.

On June 27, 1988 and August 8, 1989, two moderate-size earthquakes were located in the Lake Elsman area, at depths of 13.2 km (M_L 5.3) and 14.2 km (M_L 5.4), respectively (Olson and Hill, 1993; Dietz and Ellsworth, 1997).

The whole area is very well surveyed by a dense seismic network and seismic velocity models have been extensively tested. The Lake Elsman earthquakes were among the largest magnitudes recorded in the previous 20 years. They ruptured a secondary fault only 5 km off the Loma Prieta fault and occurred less than 4 months earlier.

The closeness in space and time of the Lake Elsman and the Loma Prieta earthquakes inspired many works dealing with coseismic stress change and also favoured the debate about coseismic stress redistribution and the feasibility of earthquake models.

Perfettini et al. (1999) addressed the problem by means of the Coulomb failure stress model. They found that Lake Elsman earthquakes should have unloaded the Loma Prieta initiation point. In their approximation, the Loma Prieta earthquake started at a location unfavoured by the stress redistribution. Perfettini et al. (1999) therefore interpreted this feature as unclamping of the Loma Prieta fault area due to the reduction of normal stress and possible fluid infusion.

In the hypothesis that Lake Elsman earthquakes can be actually related to the initiation of the Loma Prieta earthquake (as proposed by Perfettini et al., 1999), Lake Elsman–Loma Prieta time–space sequence indicates a downward propagation of seismicity, like observed in several other compressional cases.

2.3.2. The 1994 Northridge, CA, earthquake

The January 17th, 1994 Northridge Mw = 6.7 earthquake occurred on a back-thrust of a flower structure induced by the St. Andreas fault (Davis and Namson, 1994). This sequence and its foreshocks have been recorded by the dense Southern California seismic network and analysed by Hauksson et al. (1995). The mainshock was located at a depth of 19 km, at the intersection between the main thrust (Santa Monica–Elysian Park Thrust; Fig. 10) and its back thrust (Pico Thrust) and had a reverse focal mechanism on a fault plane dipping southward 35° (Hauksson et al., 1995) which exhibited up-dip directivity of the fracture (Wald et al., 1996). Aftershock seismicity was mainly shallower, located between 7 and 23 km depth and it developed not along the main thrust, but its steeper (40–45°) southwestward dipping conjugate fault, highlighting the fractured plane.

A different scenario stems from the pre-shock activity. The week before January 17, 1994 two clusters of small earthquakes occurred at distances less than 25–35 km, in areas where the background activity is rare. The Santa Monica swarm started on January 9, 1994 with a M = 3.7 earthquake, and lasted 7 days. It was located 25 km south of the Northridge epicentre, along the main Santa Monica thrust (Fig. 10). The swarm formed a tight cluster, whose radius was less than 1 km, at a depth of 3–12 km (Hauksson et al., 1995), significantly shallower than the Northridge hypocentre, and occurred on a reverse fault. Sixteen hours before the Northridge earthquake, another small cluster of 4 earthquakes occurred at a distance of 35 km, in the Holser area, at a depth of 15 km. Earthquakes were located in a volume of 1 km^2 and had a reverse mechanism. Due to the density of seismic stations, their closeness to the above described earthquakes, and the good knowledge of the velocity structure (Davis and Namson, 1994; Hauksson et al., 1995), the error on hypocentral depth estimates are less than 1 km.

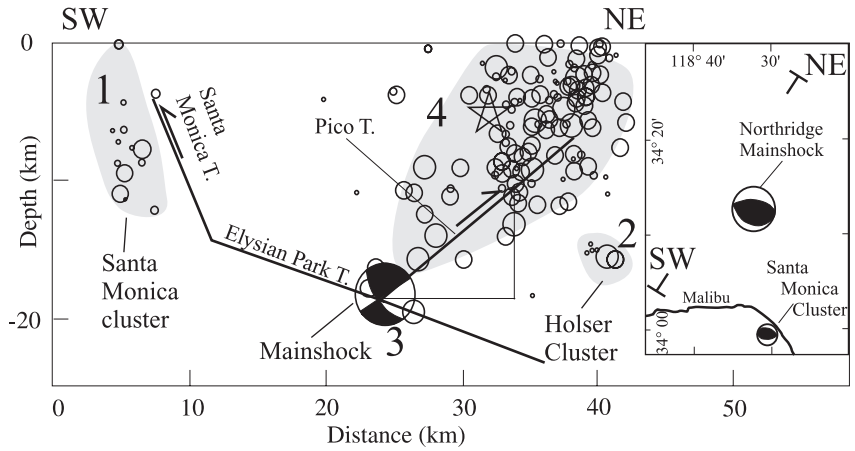

Fig. 10. Foreshocks, mainshock and aftershocks of the Northridge 1994 earthquake (redrawn and modified after Hauksson et al., 1995). On the vertical section, we display the faults recognised by Davis and Namson (1994) in a balanced geological section based on field data and oil-wells. Notice that the Santa Monica cluster most probably developed on the Santa Monica–Elysian Park main thrust. The slight misfit between this cluster and the thrust is easily explained by projection effects. The mainshock and the aftershocks developed on the Pico backthrust. The numbers in the cross-section indicate the time sequence of events or groups of events: (1) January 9–13, 1994; (2) 16 h before the mainshock; (3) Mainshock, January 17, 1994; (4) Aftershocks, first 8 h of activity after the mainshock.

The Santa Monica cluster and the Northridge mainshock occurred on two different reverse faults. However, the occurrence of the cluster in a rather aseismic area, close in space and in time to the Northridge mainshock, led Hauksson et al. (1995) to suggest a physical yet unexplained relationship between them. In fact, the Santa Monica and Northridge sequences developed in the same main thrust–back-thrust system. Because of the mechanical connection between the main thrust (Elysian–Santa Monica) and its back-thrust (Pico th.-Northridge), we suggest that the succession of Santa Monica cluster (3–12 km depth), Holser cluster (15 km), and later the Northridge mainshock (19 km) can be considered as a downward propagation of seismicity.

2.4. Contradictory observations: evidence from steeply dipping reverse faults

Although we found evidence of downward propagation of seismicity along a significantly large number of thrust faults, some well studied cases seem to contradict such observations. We selected such earthquakes with the same criteria used for the others (well-studied events, good station coverage, etc.). A list that could be also incomplete, includes: October 1, 1987, Whittier Narrows, CA (Hauksson and Jones, 1989); June 28, 1991, Sierra Madre, CA (Hauksson, 1994); and probably the January 9, 1982, New Brunswick, Canada (Choy et al., 1983). In addition, the aftershocks of 1989 Loma Prieta and 1999 Northridge events propagate upward with respect to the mainshock. Earthquake parameters of Whittier Narrows and Sierra Madre are shown in Table 1. We emphasise that these cases occurred generally along steeply dipping reverse faults. As it will be discussed in the section dedicated to the mechanical model, the fault dip parameter could provide a meaningful explanation for these observations in terms of localised supra-hydrostatic fluid pressure. Other events, like the 1976, Gazli, USSR (Hartzell, 1980) and the 1971, San Fernando, CA (Heaton, 1982), not discussed elsewhere in this work, show an upward directivity of the fracture. However, they were followed by few aftershocks nearby the fault itself and therefore cannot be used for comparison with our observations.

Some data could apparently be identified as controversial, as the 1986 Taiwan earthquake, where both upward and downward migration of seismicity has been observed (Hwang and Kanamori, 1989) or the Tennant Creek events themselves, where both phenomena are observed over adjacent fault segments (see before). Actually, these latter two cases can support the possibility that downward migration can

Table 1
Summary of compressive earthquake parameters; MS: mainshock; L: local magnitude; b: body wave magnitude; HYP: hypocenter

Site	Date	Ms	Depth (km)			Dip	Notes
			HYP	Centroid	Aftershock		
Meckering	1968, Oct 14	6.8	1	3	1–6	31–37	Model of downward fracture propagation (Vogfjörd and Langston, 1987)
Friuli	1976, May 6	6.4L	5.7	4	2–8	22	Aftershock data: Amato et al., 1976; MS data: Slejko et al., 1999
Friuli	1976, Sep 15	6.1L	11.26	5–6	5–17	38	See above
Caucete	1977, Nov 23	7.4	17 ± 5	21	15–35	35	Accurate localization of MS (Chinn and Isacks, 1983); fault dislocation model, aftershock localization (Kadinsky-Cade et al., 1985); centroid depth from Harvard database
New Brunswick	1982, Jan 9	5.7b		9 ± 1	0–7	65	Waveform modeling (Choy et al., 1983)
Nahanni	1985, Oct 5	6.5	6		2–13	30–34	Relative location of aftershocks (Wetmiller et al., 1988)
Nahanni	1985, Dec 23	6.9	6		4–15	23–25	Fracture downward directivity from near-field accelerometer data (Weichert et al., 1986)
Whittier Narrow	1987, Oct 1	5.9L	14.6		9.9–15.4	25–70	Locations: (Hauksson and Jones, 1989)
Tennant Creek	1988, Jan 22	6.3	5–8	4.5	2–6	35 S	Mainshock data (Choy and Bowman, 1990); Aftershock data: Bowman et al., 1990
Tennant Creek	1988, Jan 22	6.5	3–3.5	4.5	2–8	70 N	
Tennant Creek	1988, Jan 22	6.7	4.5	4.5	1–7	45 S	
Loma Prieta	1988, Jun 27	5.3	13.2 ± 0.8		9–12	60	"Lake Elsman"
Loma Prieta	1989, Aug 8	5.4	14.2 ± 0.8		11–14	66	"Lake Elsman"
Loma Prieta	1989, Oct 17	6.9	18 ± 1		2–19	70	(Olson and Hill, 1993; Dietz and Ellsworth, 1997)
Spitak	1988, Dec 7	6.9		5	4–8	50–55	Subevent depths by waveform modeling (Haessler et al., 1992); Temporary seismic network (Dorbath et al., 1992)
Spitak 3rd	1988, Dec 7			6	>4–10	50–55	See above
Spitak 4th	1988, Dec 7			6	5–12	50–55	See above
Racha–Dzhava	1991, Apr 29	7.0		4.8 ± 0.2	2–15	30	Subevent depths by waveform modeling (Fuenzalida et al., 1997). Aftershock data from dense local network (Triep et al., 1995; Fuenzalida et al., 1997)
Racha–Dzhava 3rd	1991, Apr 29	34		10.3 ± 0.7		60	See above
Sierra Madre	1991, June 28	5.8L	11.97		7.2–13.71	50	Locations: (Hauksson, 1994)
Northridge	1994, Jan 9	3.7L	3–12				"Santa Monica"
Northridge	1994, Jan 12	3.5L	15 ± 1				"Holser"
Northridge	1994, Jan 17	6.7	19 ± 1		7–23	35–45	(Hauksson et al., 1995)
Str. of Georgia	1997, Jun 13	3.4L	2.0		2–3		(Cassidy et al., 2000)
Str. of Georgia	1997, Jun 24	4.6L	2.7		2–3.4	47–53	(Cassidy et al., 2000)
Faenza	2000, Apr 19	3.5L	6.5		6–20		This work (Calderoni et al., 2000).
Faenza	2000, May 10	4.5L	18				See above

exist, suggesting that it can be influenced by strength heterogeneities in the crust.

3. Mechanical model

In the previous sections we showed that, along thrust faults, shallow initial ruptures and downward migration of seismicity generally occur. On the contrary, along normal faults, rupture generally occurs at deeper levels and aftershocks are shallower. Although deviations from this rule exist (some have been discussed in the previous sections), a discussion on the possible origin of such a pattern is deserved. In this section we analyse by means of Mohr diagrams simple models of rupture along normal and thrust

faults valid for isotropic bodies. In particular, we consider the variation of the vertical load along a planar fault and speculate on the consequences of this variation on the stability of faults in compressive and extensional tectonic settings since the contribution of the lithostatic load is opposite in the two regions. Our observations have been done for shallow and intermediate (0–20 km) crustal earthquakes. The presented model is intended to be valid approximately for the same depth span, i.e., between the surface and the shallower brittle–ductile transition.

Earthquakes occur by failure and relative slip of intact rocks or by reshear of pre-existing faults (Sibson, 1985, 1998). A composite failure envelope for intact isotropic rock can be constructed merging the macroscopic Griffith criterion and the Coulomb criterion for compressional shear failure (Sibson, 1998). The slope of the Coulomb envelope is controlled by the coefficient of internal friction of rocks involved in the deformation. Laboratory strength tests on several rock types showed that the internal friction coefficient ranges between 0.5 and 1.0 (Jaeger and Cook, 1979). The variation of the Coulomb envelope slope does not change our reasoning.

Reactivation of existing faults accommodates most of the deformation at the frictional seismogenic structural level (Sibson, 1983). The frictional failure envelope follows the linear Amonton's law and, for faults characterised by cohesive or cementation strength, is similar to the Coulomb envelope. The slope of the Amonton envelope is controlled by the static coefficient of friction of the fault which has been shown to have a typical value of 0.75 (Byerlee, 1978). The existence of near optimally oriented faults (at an angle close to 30° from σ_1) normally inhibits any other form of brittle failure (Sibson, 1985). As the orientation of existing faults becomes less favourable, reactivation occurs for increasingly higher effective stresses until the angle of frictional lockup is reached and Coulomb mode rupture is expected to occur.

Intact rock failure and reshear of favourably oriented existing faults are characterised, as a first approximation, by similar failure envelopes. Consequently, the following discussion holds for both cases. Reshear of unfavourably oriented faults (e.g., high-angle reverse faulting) requires localised fluid pressures significantly higher than lithostatic. Such a situation would drive to severe deviations from our simple stress distribution model, which could drive to deviations from the observed seismicity migration rule. In fact, all the compressional earthquakes showing upward migration of seismicity occurred along steep faults. At shallow depths, hydro-fracturing (due to extensional fracturing and extensional-shear fracturing) occurs in extensional regimes for lower fluid pressures than in extensional regimes. This process is considered to act as a fluid pressure regulatory mechanism (Sibson, 1981). Such a mechanism is efficient only in extensional regimes and is able to prevent the development of particularly high fluid pressures. This observation could explain the reason why the deviations from the observed seismicity migration pattern occur only in thrust faults, where super-hydrostatic fluid pressure can occur due to the inefficiency of hydro-fracturing.

Since we look for the physical model explanation of a general and simple rule, our stress distribution models must necessarily be simple. It should be taken in mind that, even if one of the presented models could represent the correct explanation to the observations, variations from our assumptions would drive to a seismic behaviour different from that described.

The following discussion assumes that the pore fluid factor λ (equal to pore fluid pressure divided by the overburden pressure) is approximately constant with depth. For sake of simplicity we adopt λ constant with depth. The choice of specific values for λ would drive to different values of σ_1 and σ_3 leaving, however, unchanged the sense of the demonstration. It should be, however, noted that major differences from model predictions would occur with λ varying significantly with depth. Overpressured compartments bounded by sealing horizons (e.g., clay rich stratigraphic horizons or impermeable faults) are typical in sedimentary basins (Hunt, 1990). In crystalline rocks the base of the upper crustal hydrostatic fluid pressure regime is likely to be limited, during interseismic periods, to the first 3–7 km (Streit and Cox, 2001). This is in agreement with recent data from deep wells. Townend and Zoback (2000) analysed in situ stress and permeability measurements from deep (down to 9.1 km) boreholes and concluded that both these datasets suggest hydrostatic fluid pressures. At depths deeper than 7–9 km, fault lithification can occur, driving to super-hydrostatic fluid pressures. These findings seem to indicate the

existence of two different shallow crustal layers in which pore fluid factors are markedly different. Most probably our reasoning is valid if only one of the two tectonic levels is considered at a time. It should be moreover noted that earthquakes should preferentially occur in the deeper level, where super-hydrostatic fluid pressures should be reached. This is compatible with observations. The shallowest earthquakes described in previous sections were shown to have nucleated at depths greater than 3–5 km.

3.1. State of stress in extensional and compressional regimes

It is widely accepted that the vertical stress coincides with the lithostatic load, equal to $\sigma_v = \rho g h (1-\lambda)$, where ρ is the rock density, g is the gravity acceleration and h is the depth. Less clear is the change of horizontal stresses with depth. The non-tectonic state of stress for the uppermost crust is still matter of debate (e.g., McGarr, 1987, 1988; Leary, 1987). Two different theoretical models have been proposed to describe the horizontal non-tectonic stress. Several researchers have proposed mechanical models assuming that non-tectonic horizontal stress varies as $\sigma_h = [\nu/(1-\nu)]\sigma_v$ (Poisson effect, see e.g., Twiss and Moores, 1992), where ν is the Poisson's ratio (values between 0.25 and 0.33 are common for rocks). According to this relation, assuming $\nu = 0.25$, the non-tectonic component of horizontal stress is $\sigma_v/3$. As shown in Fig. 11a, σ_h grows more slowly than σ_v with depth. This relation is based on the assumption that the uppermost brittle crust behaves elastically and upper crustal rocks are laterally constrained (and therefore the horizontal strain is imposed equal to zero). Since we deal with the shallow brittle portion of the crust, such assumptions seem to be reasonable. However, the validity of this 'lateral constraint' state of stress has been first questioned by Anderson (1951), who suggested that over long time periods the crust deforms inelastically in response to any deviatoric stress and thus tends to the state for which there is no deviatoric stress. This implies that $\sigma_v = \sigma_h = \rho g h (1-\lambda)$ (McGarr, 1988). We expect that this stress distribution better applies to weaker rocks at deeper levels, where the stress isotropic behaviour is restored, leading to a non-tectonic stress distribution with depth similar to that shown in Fig. 12a.

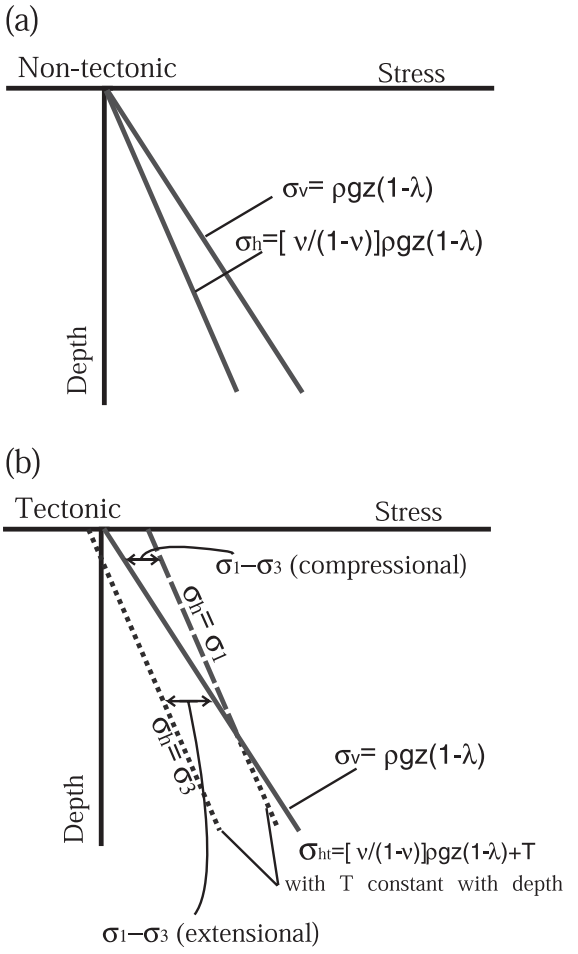

Fig. 11. Distribution of stress in absence (a) and in presence (b) of tectonic loads assuming a 'lateral constraint' state of stress and constant tectonic stresses with depth.

In the following, we discuss the implications of these two simplified non-tectonic states of stress on rupture location. The tectonic state of stress (σ_{ht}) is here considered, as a first approximation, to be equal to $\sigma_{ht} = [\nu/(1-\nu)]\ \rho g h(1-\lambda) + T$ and to $\sigma_{ht} = \rho g h(1-\lambda) + T$ for the 'lateral constraint' and for the 'no lateral constraint' states of stress, respectively. T is the tectonic component of the horizontal stress, positive for compressional and negative for tensional cases, and is, as a first approximation, assumed to be constant with depth. Figs. 11b and 12b show the stress distribution with depth in the presence of applied constant tectonic forces for the 'lateral con-

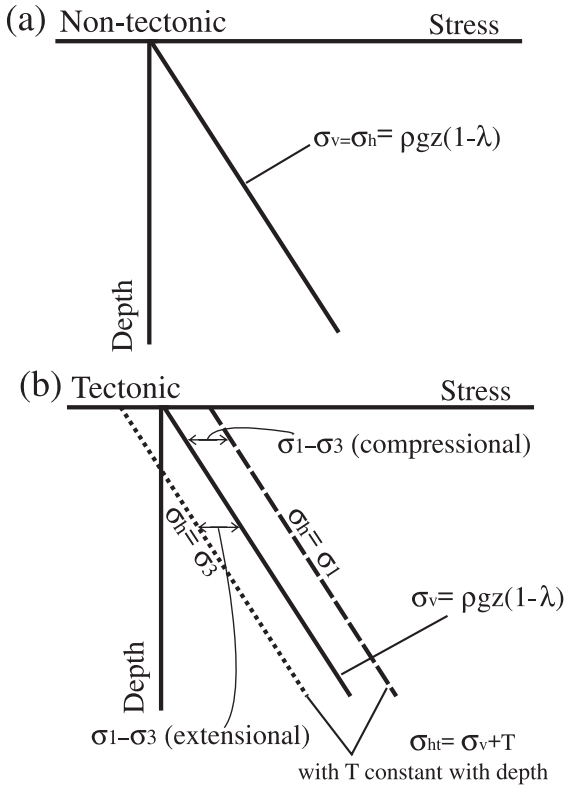

Fig. 12. Distribution of stress in the absence (a) and in the presence (b) of tectonic loads assuming a 'no lateral constraint' state of stress and constant tectonic stresses with depth.

straint' and for the 'no lateral constraint' cases, respectively. It should be noticed that in Fig. 11b the differential stress (equal to $\sigma_1 - \sigma_3$, i.e., the horizontal distance between full and dotted or dashed lines) increases with depth in extensional regimes and diminishes in compressional regimes. On the contrary the differential stress remains constant with depth for both regimes in Fig. 12b.

3.2. State of stress and earthquake nucleation depth

To clarify the effects of the stress distributions of Figs. 11 and 12 on earthquake nucleation depths in extensional and compressional regimes, the Mohr circle representation is used. Here the state of stress of two points (A and B) positioned at increasing depths along hypothetical thrust and normal faults is discussed (Figs. 13 and 14).

According to the Anderson fault theory, the lithostatic load, coincident with the vertical stress, is the minimum stress axis in compressional settings, while it is the maximum stress axis in extensional settings. Since A is shallower than B, the vertical load increases from point A to point B.

In compressional regimes, the vertical load is σ_3. As far as the 'lateral constraint' state of stress is considered, moving upward from location B to A, the differential stress (the diameter of the Mohr circle) increases (Fig. 13a). As a consequence, moving upward along a thrust fault, the decrease of σ_3 enlarges the Mohr circle making the fault plane more unstable. This means that rupture along the fault is likely to occur at shallower depths and that both the fracture and early aftershocks are expected to propagate downward, consistently with observations outlined above. On the other hand, if a small earthquake occurs at greater depths, it is unlikely to propagate upward and to grow into a larger one. Such a model seems to be consistent with observations of seismicity induced in oil fields in the western US (McGarr, 1991). In fact, oil extraction seems to be responsible for a decrease in the vertical lithostatic load (which coincides in compressional regimes with σ_3). This increases the differential stress, enlarging the Mohr circle, and ultimately it might determine an increment in the seismicity associated to active thrust faults.

In extensional regimes, the opposite occurs. The vertical load is σ_1. Moving from location B to A, the differential stress decreases (Fig. 11b). The decrease of σ_1 diminishes the Mohr circle making the fault plane more stable at shallower depth (Fig. 13b). As a consequence rupture is expected to occur, along normal faults, at deeper depths and early aftershocks are expected to propagate upwards, as observed in natural cases. In such a scenario, changes of the tectonic component of stress with depth could drive to deviations from the above-described seismic behaviour. However, it is clear that a 'lateral constraint' non-tectonic state of stress would justify a preference for shallow and deep rupture along thrust and normal faults, respectively.

In the frame of the 'no lateral constraint' state of stress, for our simplistic assumption of tectonic stress, we should expect differential stresses constant with depth. In both thrust and normal faulting regimes,

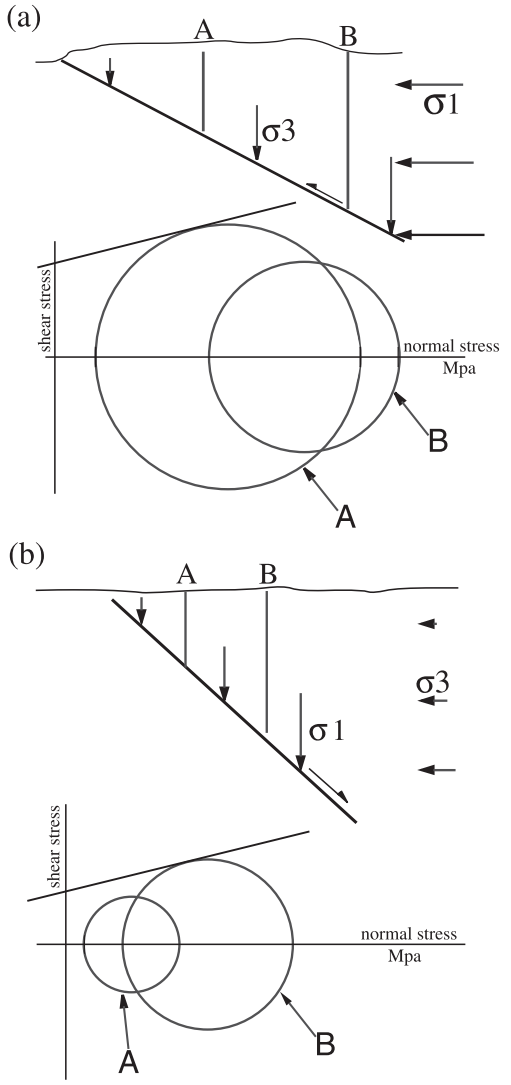

Fig. 13. (a) Sketch and Mohr diagrams of the variation of σ_3 (vertical load) and σ_1 (horizontal load) along thrust faults according to the 'lateral constraint' state of stress shown in Fig. 11. (b) Sketch and Mohr diagram of the variation of σ_1 (vertical load) and σ_3 (horizontal load) along normal faults according to the 'lateral constraint' state of stress shown in Fig. 11.

when moving from point A to point B, the Mohr circle moves to the right maintaining its diameter constant (Fig. 14a,b) This would drive to no contrasting seismic behaviour along thrusts and normal faults. Since our assumption of tectonic stress constant with depth is likely to fail in natural cases, a random increase or decrease of the tectonic stress with depth would randomly control the rupture depth. In such a scenario an alternative explanation for the contrasting behaviour of seismicity in compressional and extensional regimes should be looked for.

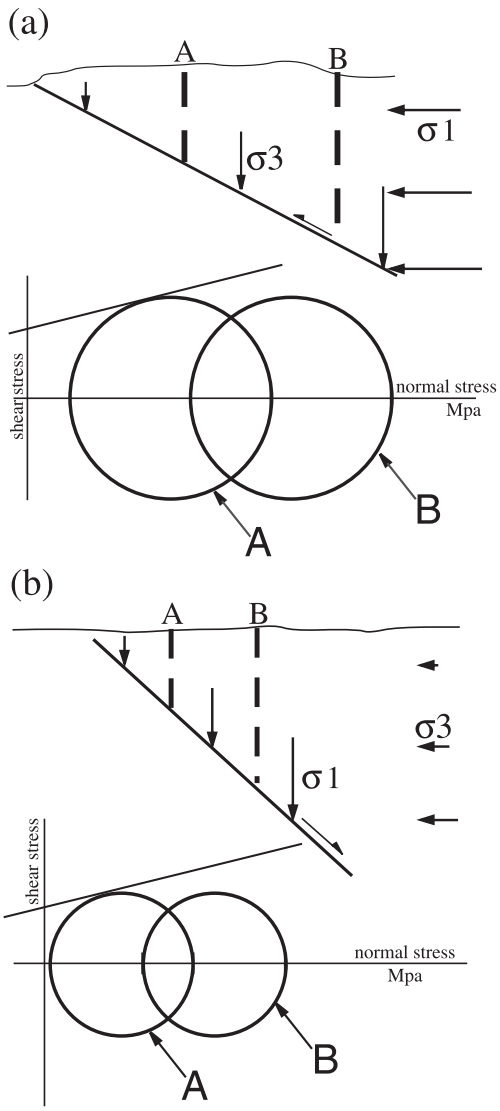

Fig. 14. (a) Sketch and Mohr diagrams of the variation of σ_3 (vertical load) and σ_1 (horizontal load) along thrust faults according to the 'no lateral constraint' state of stress shown in Fig. 12. (b) Sketch and Mohr diagram of the variation of σ_1 (vertical load) and σ_3 (horizontal load) along normal faults according to the 'no lateral constraint' state of stress shown in Fig. 12.

4. In situ stress measurements

Although the stress distribution models described above have been considered reasonably realistic in the literature, very little is known about the distribution of stress with depth. Stress measurements in boreholes have been performed in several areas in the world. Some of the measurement results are shown in Fig. 15. It should be emphasised that most borehole measurements were performed at depths ranging from 0 to 4–5 km, whereas most of the earthquakes described above originated at deeper depths. Measurements down to 9 km are available only for the KTB well (Brudy et al., 1997), drilled in a strike slip tectonic regime.

In extensional settings (Fig. 15a,b) from US and South Africa (McGarr and Gay, 1978), stress measurements indicate a slower increase of horizontal stress with respect to vertical stress which drives to an increase of differential stress with depth qualitatively similar to that shown in Fig. 11b. Such a stress distribution seems compatible with the seismological observations outlined above.

A recent review of in situ stress measurements (Townend and Zoback, 2000) shows that, for six boreholes from different locations in the world, the differential stress grows regularly with depth according to the Coulomb frictional failure theory (Fig. 15e). It should be, however, emphasised that the six wells analysed by Townend and Zoback (2000) were drilled in extensional (Dixie Valley and Fenton Hill) and strike slip (Cornwall, Cajon Pass, Siljan and KTB)

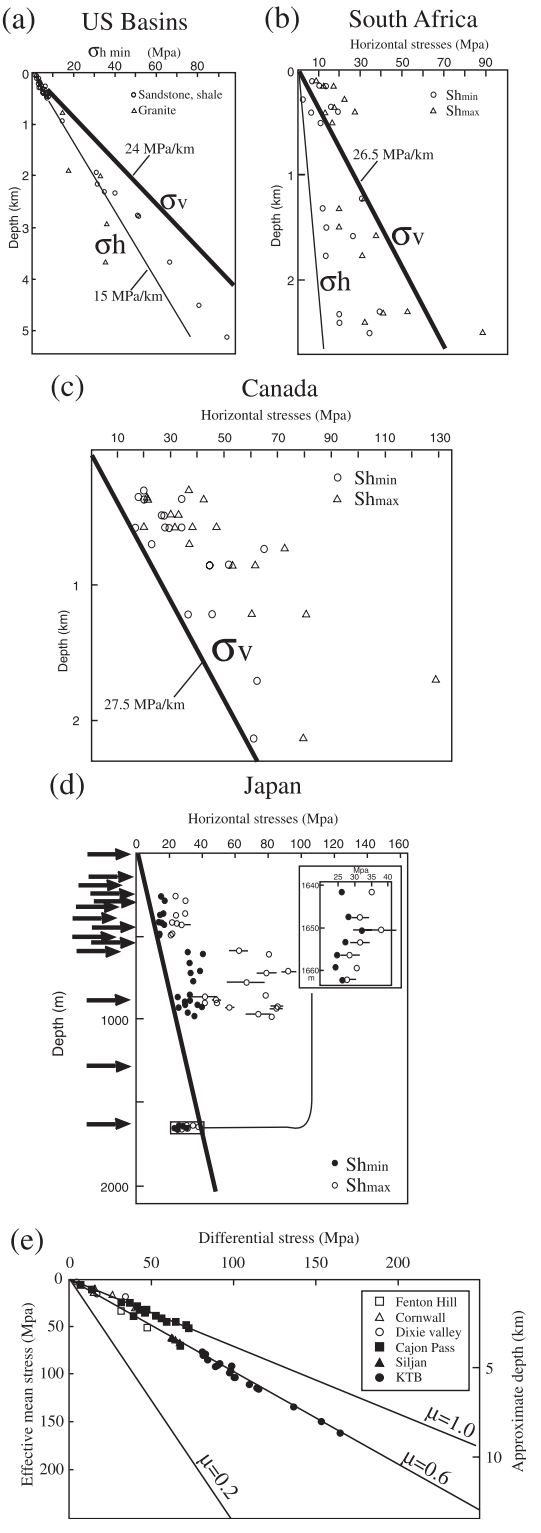

Fig. 15. Borehole stress measurements performed in extensional regimes (a,b) and in compressional regimes (c) (redrawn and modified after McGarr and Gay, 1978). Triangles and circles in panel (a) represent horizontal stress measurements performed in sandstones/shales and in granites, respectively. Triangles and circles in panel (b,c) represent measurements of maximum and minimum horizontal stresses, respectively. (d) Borehole stress measurements performed in the Oshio seismic zone (Japan). Large arrows indicate the position of the faults cross-cut by the well (redrawn and modified after Tsukahara et al., 1996). Circles and dots represent measurements of maximum and minimum horizontal stresses, respectively. (e) Stress data from six deep boreholes (drilled in extensional and strike slip environments) distributed world-wide are plotted in order to show the dependence of differential stress on effective mean stress. The solid lines show the relationship predicted by Coulomb frictional failure theory for friction coefficients of 0.2, 0.6 and 1.0 (redrawn and modified after Townend and Zoback, 2000).

tectonic environments. The increase of differential stress with depth in extensional regimes is compatible with our seismological observations. Unfortunately, Fig. 15e does not shed light on the variation of the magnitude of differential stress with depth in compressional environments.

Available stress measurements in compressional regimes (Fig. 15c,d) are difficult to interpret. No simple rules can be extracted. Very little inference can be obtained on the variation of differential stress with depth. However, some considerations deserve to be done; the stress distributions from borehole measurements were determined in hydrostatic fluid pressure regimes (at shallow depths). Therefore they cannot simply be extrapolated to deeper depths where super-hydrostatic fluid pressure can occur (Streit and Cox, 2001). Moreover, Tsukahara et al. (1996) have shown that borehole measurements performed in the Ashio seismic zone (Japan) showed strong variations of differential stresses when the well intersects an active fault (Fig. 15d). As a consequence, stress measurements performed far from active faults seem to be not representative of the stress field nearby active faults. These considerations cast doubts on the possibility to use measurements displayed in Fig. 15c,d to reconstruct the stress field at depth in the vicinity of faults in active areas.

Analysing the stress measurements of Fig. 15e, Townend and Zoback (2000) conclude that the seismogenic crust is in a state of frictional failure equilibrium. This conclusion is supported, according to Zoback and Townend (2001), by other lines of evidence, such as seismicity induced by fluid injection and triggered by previous earthquakes. Following this view, small changes of the crustal state of stress induced by these processes would drive to rupture. Townend and Zoback (2000) show that differential stress increases with depth for normal and strike slip faults and should reach maximum values at the base of the seismogenic crust. If frictional–brittle and ductile layers of the crust are coupled, the base of the frictional crust should accommodate the deformation occurring by aseismic slip within the ductile level. These considerations led some authors (Das and Scholz, 1983; Sibson, 1983) to suggest that moderate to large earthquakes tend to nucleate near the base of the brittle layer, the region inferred to have the highest shear resistance and concentration of distorsional strain energy. This is compatible with our seismological observations on normal faults.

As already discussed, no precise information is available on the state of stress in compressional environments. A compressional state of stress similar to that shown in Fig. 15e, i.e., differential stresses progressively larger with depth, would be difficult to reconcile with the prevalence of shallow nucleation of earthquakes along thrusts. It should be noticed, on the contrary, that a crustal state of stress close to frictional failure equilibrium could account for the variety of behaviour occurring in compressional regimes.

Fig. 16 represents a synthesis of the reasoning so far. In extensional regimes, the differential stress is likely to increase with depth, accordingly to theoretical considerations and to in situ stress measurements. This induces a preference for deep rupture and upward migration of seismicity, consistently with our seismological observations and with previous works (Das and Scholz, 1983; Sibson, 1983). The situation is more blurred for compressional regimes. Tentatively, Fig. 16 displays a possible variation of differential stress with depth in such regimes. The above-discussed shallow ruptures along thrust faults could be related to a general tendency to differential stress

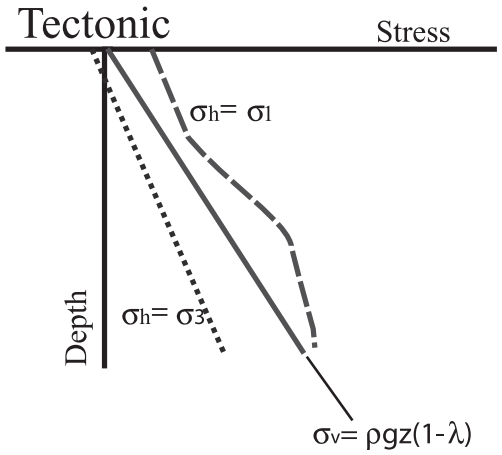

Fig. 16. Cartoon of a possible distribution of stress in presence of applied tectonic loads as inferred from borehole measurements and considerations done in the text. The solid line represents the vertical lithostatic load. The dotted line is the horizontal stress in compressional environments. The dashed line represents the horizontal stress in extensional tectonic settings.

decrease with depth in compressional regimes. Deviations from this tendency, sketched in Fig. 16, possibly enhanced by a state of stress close to frictional failure equilibrium, could drive to rupture at deeper depth. We think that these deviations are more likely to occur near the base of the seismogenic layer, where nucleation of large compressional earthquakes has already been explained (Sibson, 1982; Das and Scholz, 1983). Moreover, such deviations are likely to be more frequent in areas characterised by high variability both in space and time of the tectonic signature. Tectonics in southern California is controlled by the strike slip motion along the San Andreas fault system. However, transtensional and transpressional deformation occurs in several closely spaced locations. The state of stress in transpressional areas could differ significantly from that of purely compressional environments. This could explain our seismological observations, i.e., that all of the deep nucleations along thrust faults occurred in California. Moreover, the stress field in California is disturbed by extensional tectonics, particularly evident in the Basin and Range but also reaching the Californian region.

5. The role of topography

We have shown above that the different role of the vertical lithostatic load in extensional and compressional tectonic settings could possibly control rupture location and seismicity migration. Since topography contributes to the vertical loads, this could imply that topography could have a direct control on seismicity style as well.

Let us consider a rock volume at a fixed depth with respect to mean sea level. Higher and lower vertical lithostatic loads will act on this rock volume for higher and lower topographic elevations,

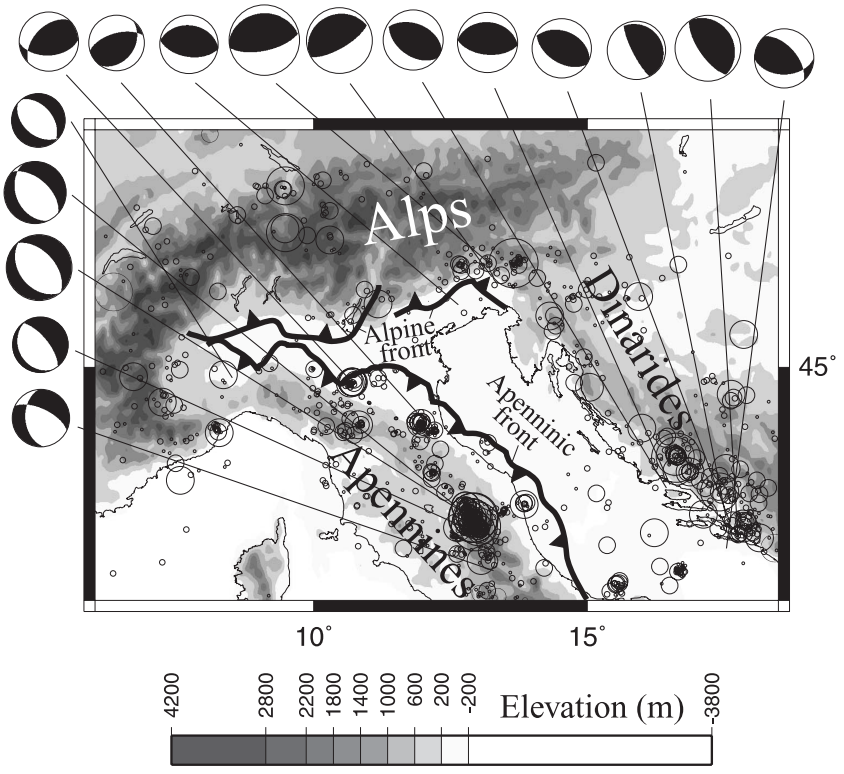

Fig. 17. Elevation, seismicity and focal mechanisms of main seismic events in the Italian area. Notice that large extensional earthquakes occur along the Apennines backbone and correspond to high elevations. Compressional earthquakes develop at the border of the Alps and at the northernmost–easternmost border of the Apennines in correspondence to low elevations. Data from INGV.

respectively, leaving horizontal loads approximately constant.

In compressional environments, high elevations would increase the minimum vertical stress and low elevations would reduce the minimum stress. This would result in a decrease and in an enlargement of the Mohr circle in the two cases, respectively. As a consequence, high topography should inhibit the occurrence of large compressional earthquakes, which should preferably occur in areas of low relief. On the contrary, in extensional environments high elevation would increase the maximum (vertical) stress (increasing the differential stress) and low elevation would reduce the maximum stress (decreasing the differential stress). Consequently, we would expect extensional earthquakes to occur preferably in areas with high topography.

As possible examples of this process we discuss topography and seismic distribution of northern Italy and surroundings (Fig. 17), central Andes (Fig. 18) and Himalaya (Fig. 19). The Tertiary and Quaternary geology of Italy is controlled by three processes: (i) the 'eastward' roll back of the hinge of the west directed subduction of the Adriatic plate driving to the formation of the Apenninic belt and to the opening of the Tyrrhenian sea (e.g., Malinverno and Ryan, 1986); (ii) the southeastward subduction of the European plate underneath the Adriatic plate in correspondence of the Alps, driving to the development of the Alpine chain; (iii) the northeastward directed subduction of the Adriatic plate underneath Eurasia to form the Dinarides. As shown in Fig. 17, the seismicity along the Apennines is mainly extensional and large to moderate in magnitude in the internal part of the

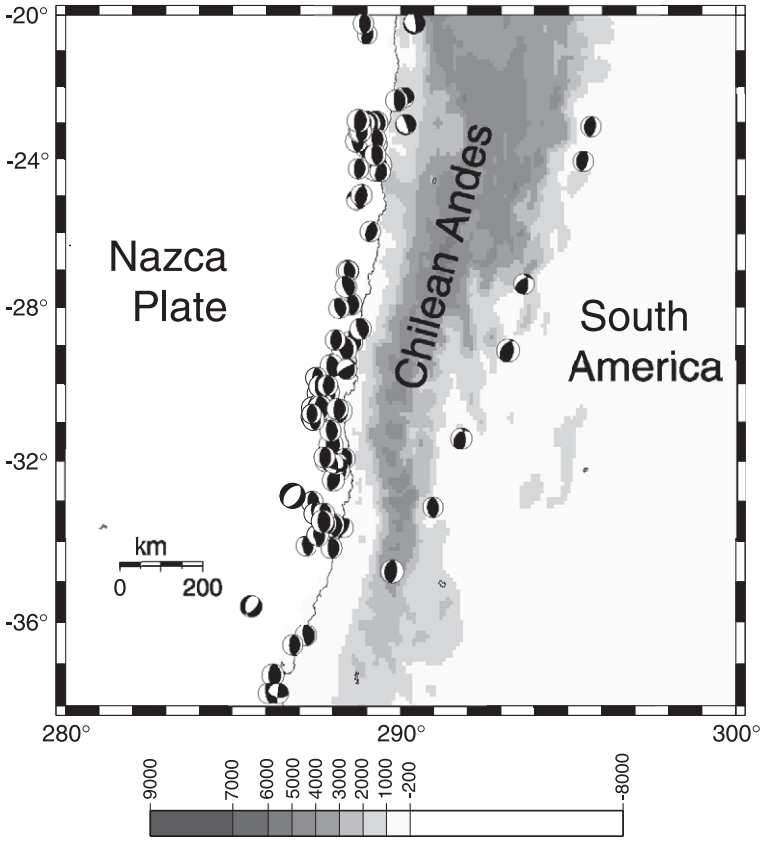

Fig. 18. Elevation and focal mechanisms of main seismic events (occurred between 1990 and 2003 and at depth ranging from 0 to 33 km) in the central Andean area. Notice that compressional earthquakes develop at the border of the Andes, both in the pro- and in the retro-belt, in correspondence to low elevations. Data from the Harvard CMT catalogue (Harvard, 2003).

chain, in correspondence with the highest elevations. On the contrary, moderate to small compressional earthquakes develop in the northernmost and easternmost external portions of the chain (Frepoli and Amato, 1997; Frepoli and Amato, 1999), buried underneath the low relief foreland basins of the Po Plain and the Adriatic Sea. In the Alps, large to moderate compressional earthquakes occur mainly at the northern and southern borders of the chain, along thrusts buried underneath the sediments of the Po Plain and of the Molasse foreland basins. Extensional earthquakes occur along the axis of the chain in correspondence of the highest elevations. Compressive earthquakes occur at the front of the Dinarides in areas of low elevation, in the eastern side of the Adriatic Sea (Fig. 17).

The Cenozoic to Present tectonics of the Andean region are induced by the east-directed subduction of the Nazca oceanic plate under the South America continental plate (Reutter et al., 1994). The focal mechanisms of major earthquakes occurred in the central Chilean Andes region from 1990 to 2003 are displayed in Fig. 18. These earthquakes occurred along reverse faults and are located at the low topography fronts of the forebelt and retrobelt of the Andes.

Fig. 19 shows the focal mechanisms of major earthquakes occurred in the Himalayan region between 1980 and 2003. The Tertiary to Present tectonics are governed by the collision between the India and Asia plates (Windley, 1995). Reverse, normal and strike slip earthquakes are widespread in the area.

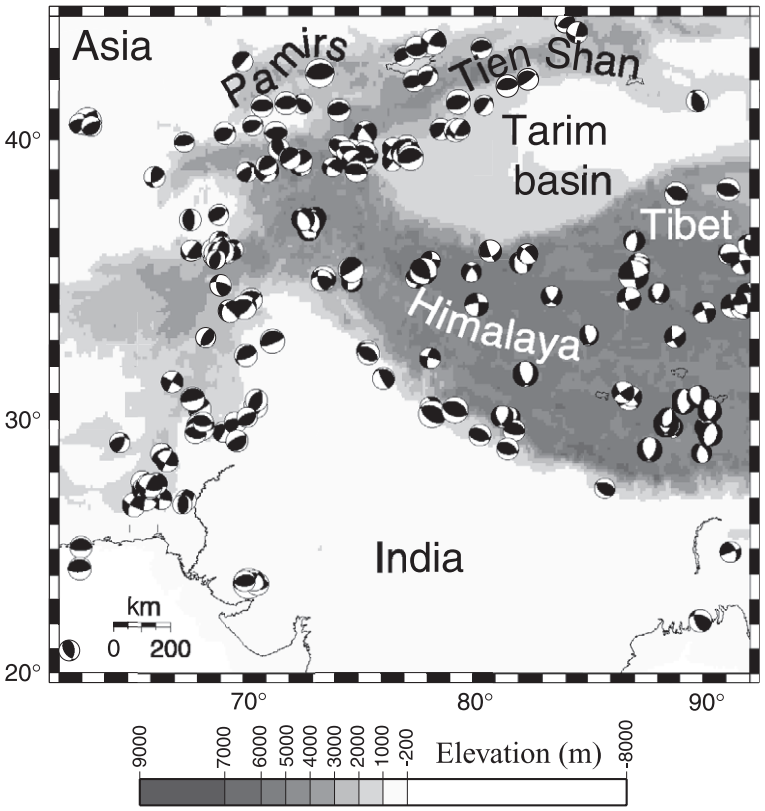

Fig. 19. Elevation and focal mechanisms of main seismic events (occurred between 1980 and 2003 and at depth ranging from 0 to 20 km) in the Himalayian area. Compressional earthquakes are mainly concentrated at the northern and southern borders of the chain, in correspondence to low elevations. Most of extensional earthquakes are located in the axial part of the mountain belt, in correspondence with high elevations. Data from the Harvard CMT catalogue (Harvard, 2003).

Although the earthquakes pattern is more complex than in the previous cases, some common features can be outlined. Most of the compressional earthquakes occur at the southern border of the Himalayas, at the southern and northern borders of the Tien Shan and around the Pamirs, in correspondence of low topography areas. With a few exceptions, the high elevation areas of Himalaya and Tibet are characterised by extensional earthquakes.

The location of earthquakes is controlled by several factors, such as geodynamic processes, local tectonic features, rock rheology. Moreover, these and other processes control also the stress distribution and the tectonic regime (compressional, extensional or strike slip). However, the seismological observations of Figs. 17, 18 and 19 confirm our expectation of compressional shallow earthquakes being prevalent in low elevation and extensional earthquakes occurring mostly in high elevation zones. Further work is however needed to better evaluate the control of topography on earthquake distribution.

6. Conclusions

We consider several earthquakes available in literature occurred in extensional and compressional tectonic realms and show that shallow rupture and downward migration of seismicity preferentially occur along thrust faults, whereas rupture generally occurs at deeper levels and aftershocks are shallower along normal faults.

We suggest that the contrasting seismic behaviour of thrust and normal faults can possibly be related to the inversion of the role of the lithostatic load in the two fields, i.e., it is the minimum stress in compressional regimes, the maximum in extensional regimes. This could determine, in absence of localised fluid overpressures, an increase of differential stress with depth in extensional regimes and a decrease in compressional regimes. Therefore, assuming commonly accepted brittle/frictional fracture criteria, if this stress distribution is valid, we may expect opposite propagation of rupture and early aftershocks in compressional and extensional tectonic fields, consistently with observations. We show that exceptions to the downward migration of seismicity along thrust faults occur on steeply inclined faults and imply the occurrence of localised supra-lithostatic fluid pressures.

A further consequence of the inversion of the meaning of the lithostatic load regards the role of topography. High topography, increasing the vertical load, should inhibit earthquake development in compressional environments and enhance it in extensional settings. Although factors such as geodynamic processes, local tectonic features, and rock rheology may complicate this simple scenario, these model predictions are consistent with seismicity distribution in Italy, central Andes and Himalaya.

Acknowledgements

We thank G. De Natale, G. Panza, P. Harabaglia, A. McGarr, R. Sibson and S. Nielsen for fruitful discussions and Y. Nakamura for comments on the manuscript. Two anonymous reviewers and the editor are acknowledged for their accurate and useful comments. ASI 2001, Cofin 2001 and GNDT fundings (C. Doglioni) are acknowledged.

References

Aki, K., 1992. Higher-order interrelations between seismogenic structures and earthquake processes. Tectonophysics 211, 1–12.

Amato, A., Barnaba, P.F., Finetti, I., Groppi, G., Martinis, B., Muzzin, A., 1976. Geodynamic outline and seismicity of Friuli Venetia Julia region. Boll. Geofis. Teor. Appl., XIX 72, 217–256.

Amato, A., Selvaggi, G., 1993. Aftershock location and P-velocity structure in the epicentral region of the 1980 Irpinia earthquake. Ann. Geofis. 36, 3–15.

Anderson, E.M., 1951. The Dynamics of Faulting and Dyke formation with application to Britain, 2nd ed. Oliver and Boyd, Edinburgh.

Barba, S., Basili, R., 2000. The analysis of seismological and geological observations for moderate sized earthquakes: the Colfiorito fault system (Central Apennines, Italy). Geophys. J. Int. 141, 241–252.

Bernard, P., Zollo, A., 1989. The Irpinia (Italy) 1980 earthquake: detailed analysis of a complex normal fault. J. Geophys. Res., B 94, 1631–1648.

Biagi, P.F., Caloi, P., Migani, M., Spadea, M.C., 1976. Tilting variations and seismicity that preceded the strong Friuli earthquake of May 6th, 1976. Ann. Geofis. 29 (3), 137–145.

Boschi, E., Guidoboni, E., Farrari, G., Valensise, G., Gasperini, G., 1997. Catalogo dei forti terremoti in Italia dal 461 a.C. al 1990. Istituto Nazionale di Geofisica, Roma.

Bowman, J.R., 1988. Constraints on locations of large intraplate earthquakes in the Northern Territory, Australia from observations at the Warramunga seismic array. Geophys. Res. Lett. 15, 1475–1478.

Bowman, J.R., Dewey, J.W., 1991. Relocation of teleseismically recorded earthquakes near Tennant Creek, Australia; implications for midplate seismogenesis. J. Geophys. Res., B 96, 11973–11979.

Bowman, J.R., Gibson, G., Jones, T., 1990. Aftershocks of the 1988 January 22 Tennant Creek, Australia intraplate earthquakes; evidence for a complex thrust-fault geometry. Geophys. J. Int. 100, 87–97.

Braitenberg, C., Zadro, M., 1999. The Grotta Gigante horizontal pendulums—instrumentation and observations. Boll. Geofis. Teor. Appl. 40, 577–582.

Brudy, M., Zoback, M.D., Fuchs, K., Rummel, F., Baumgaertner, J., 1997. Estimation of the complete stress tensor to 8 km depth in the KTB scientific drill holes: implications for crustal stress. J. Geophys. Res., B 102, 18453–18475.

Byerlee, J.D., 1978. Friction of rocks. Pure Appl. Geophys. 116, 615–626.

Calderoni, G., Azzara, R., Cattaneo, M., Di Bona, M., Mele, F., Selvaggi, G., 2000. Analisi preliminare della sequenza del Forlivese (Aprile–Maggio 2000). Proceedings of XIX GNGTS Meeting. CNR, Rome, p. 242.

Caloi, P., Spadea, M.C., 1955. Relazioni fra lente variazioni di inclinazione e moti sismici in zona ad elevata sismicit. Rc. Accad. Naz. Lincei, Ser. 8 (18), 250–256.

Cassidy, J.F., Rogers, G.C., Waldhauser, F., 2000. Characterization of active faulting beneath the Strait of Georgia, British Columbia. Bull. Seismol. Soc. Am. 90, 1188–1199.

Chinn, D.S., Isacks, B.L., 1983. Accurate source depths and focal mechanisms of shallow earthquakes in Western South America and in the New Hebrides Island Arc. Tectonics 2, 529–563.

Choy, G.L., Boatwright, J., 1988. Teleseismic and near-field analysis of the Nahanni earthquakes in the northwestern territories, Canada. Bull. Seismol. Soc. Am. 78, 1627–1652.

Choy, G.L., Bowman, J.R., 1990. Rupture process of a multiple main shock sequence; analysis of teleseismic, local, and field observations of the Tennant Creek, Australia, earthquakes of January 22, 1988. J. Geophys. Res., B 95, 6867–6882.

Choy, G.L., Boatwright, J., Dewey, J.W., Sipkin, S.A., 1983. A teleseismic analysis of the New Brunswick earthquake of January, 9, 1982. J. Geophys. Res. 88 (B), 2199–2212.

Chrone, A.J., Machette, M.N., Bonilla, M.G., Lienkaemper, J.J., Pierce, K.L., Scott, W.E., Bucknam, R.C., 1987. Surface faulting accompanying the Borah Peak earthquake and segmentation of the Lost River Fault, central Idaho. Bull. Seismol. Soc. Am. 77, 739–770.

Cisternas, et al., 1989. The Spitak (Armenia) earthquake of December 1988; field observations, seismology and tectonics. Nature 339, 675–679.

Das, S., Scholz, C.H., 1981. Off-fault aftershock clusters caused by shear stress increase? Bull. Seismol. Soc. Am. 71, 1669–1675.

Das, S., Scholz, C.H., 1983. Why large earthquakes do not nucleate at shallow depth. Nature 305, 621–623.

Davis, T.L., Namson, J.S., 1994. A balanced cross-section of the 1994 Northridge earthquake, Southern California. Nature 372, 167–169.

Dewey, J.W., 1984. Analysis of the seismicity of central Idaho using data from the Borah Peak earthquake sequence of 1983. EOS, Trans. Am. Geophys. Union 65, 13–17.

Dietz, L.D., Ellsworth, W.L., 1990. The October 17, 1989, Loma Prieta, California, earthquake and its aftershocks: geometry of the sequence from high-resolution locations. Geophys. Res. Lett. 17, 1417–1420.

Dietz, L.D., Ellsworth, W.L., 1997. Aftershocks of 1989 Loma Prieta earthquake and their tectonic implications. In: Reasemberg, P.A. (Ed.), The Loma Prieta, California, Earthquake of October 17, 1989—Aftershocks and postseismic effects. U.S. Geol. Surv. Prof. Paper, vol. 1550-D, pp. 5–48.

Doglioni, C., 2000. Sismotettonica dell'Italia nord-orientale e possibile comparazione con gli Appennini. In: Galadini, F., Melleti, C., Rebez, A. (Eds.), Le ricerche del GNDT nel campo della pericolosita' sismica (1996–1999). CNR-Gruppo Nazionale Difesa Terremoti, Roma, pp. 51–58.

Dorbath, L., Dorbath, C., Rivera, L., Fuenzalida, A., Cisternas, A., Tatevossian, R., Aptekman, J., Arefiev, S., 1992. Geometry, segmentation and stress regime of the Spitak (Armenia) earthquake from the analysis of the aftershock sequence. Geophys. J. Int. 108, 309–328.

Doser, D.I., Smith, R.B., 1995. Source parameters of the 28 October 1983 Borah Peak, Idaho, earthquake from body wave analysis. Bull. Seismol. Soc. Am. 75, 1041–1051.

Dragoni, M., Bonafede, M., Boschi, E., 1985. On the interpretation of slow ground deformation precursory to the 1976 Friuli earthquake. Pure Appl. Geophys. 122 (6), 781–792.

Everingham, I.B., Gregson, P.J., Doyle, H.A., 1969. Thrust fault scarp in the Western Australian shield. Nature 223, 701–703.

Fisher, M.A., et al., 1999. Seismic survey probes urban earthquake hazards in Pacific Northwest. EOS, Trans. Am. Geophys. Union 80, 13–17.

Fredrich, J., McCaffrey, R., Denham, D., 1988. Source parameters of seven large Australian earthquakes determined by body waveform inversion. Geophys. J. Int. 95, 1–13.

Frepoli, A., Amato, A., 1997. Contemporaneous extension and compression in the northern Apennines from earthquake fault plane solution. Geophys. J. Int. 129, 368–388.

Frepoli, A., Amato, A., 1999. Fault plane solution of crustal earthquakes in southern Italy (1988–1995): seismotectonic implications. Ann. Geofis. 43, 437–467.

Fuenzalida, H., Rivera, L., Haessler, H., Legrand, D., Philip, H., Dorbath, L., McCormack, D., Arefiew, S., Langer, C., Cisternas, A., 1997. Seismic source study of the Racha–Dzhava (Georgia) earthquake from aftershocks and broad-band teleseismic body-wave records: an example of active nappe tectonics. Geophys. J. Int. 130, 29–46.

Giardini, D., 1996. Teleseismic observation of the November 23 1980. Irpinia earthquake. Ann. Geofis. 36 (1), 17–25.

Haessler, H., Deschamps, A., Dufumier, H., Fuenzalida, H., Cisternas, A., 1992. The rupture process of the Armenian earthquake from broad-band teleseismic body wave records. Geophys. J. Int. 109, 151–161.

Harris, R., 1998. Introduction to special section: stress triggers, stress shadows, and implications for seismic hazard. J. Geophys. Res., B 103, 24347–24358.

Hartzell, S.H., 1980. Faulting process of the May 17, 1976, Gazli, USSR earthquake. Bull. Seismol. Soc. Am. 70, 1715–1736.

Harvard, 2003. http://www.seismology.harvard.edu/CMTsearch.html.

Hauksson, E., 1994. The 1991 Sierra Madre earthquake sequence in Southern California: seismological and tectonic analysis. Bull. Seismol. Soc. Am. 84, 1058–1074.

Hauksson, E., Jones, L.M., 1989. The 1987 Whittier Narrows earthquake sequence in Los Angeles, Southern California: seismological and tectonic analysis. J. Geophys. Res. 94B, 9569–9589.

Hauksson, E., Jones, L., Hutton, K., 1995. The 1994 Northridge earthquake sequence in California; seismological and tectonic aspects. J. Geophys. Res., B 100, 12335–12355.

Heaton, T.H., 1982. The 1971 San Fernando earthquake: a double event? Bull. Seismol. Soc. Am. 72, 2037–2062.

Hunt, J.M., 1990. Generation and migration of petroleum from abnormally pressured fluid compartments. Am. Assoc. Pet. Geol. Bull. 74, 1–12.

Hwang, L.J., Kanamori, H., 1989. Teleseismic and strong-motion source spectra from two earthquakes in eastern Taiwan. Bull. Seismol. Soc. Am. 79, 935–944.

Jaeger, J.C., Cook, N.G.W., 1979. Fundamentals of Rock Mechanics, 3rd ed. Mathuen, London. 593 pp.

Kadinsky-Cade, K., Reilinger, R., Isacks, B., 1985. Surface deformation associated with the November 23, 1977, Caucete, Argentina, earthquake sequence. J. Geophys. Res. 90 (B), 12691–12700.

Leary, P.C., 1987. Reply to ‘‘Comments on ‘Near-surface stress and displacement in a layered elastic crust’ and ‘Stress in a stratified crust overlying a buried screw dislocation’ by P.C. Leary’’ by A. McGarr. J. Geophys. Res., B 92, 4965–4969.

Lettis, W.R., Wells, D.L., Baldwin, J.N., 1997. Empirical observations regarding reverse earthquakes, blind thrust faults, and quaternary deformation: are blind thrust faults truly blind? Bull. Seismol. Soc. Am. 87, 1171–1198.

Malinverno, A., Ryan, W.B.F., 1986. Extension in the Tyrrhenian sea and shortening in the Apennines as a result of arc migration driven by sinking of lithosphere. Tectonics 5, 227–245.

McGarr, A., 1987. Comments on ‘‘Near-surface stress and displacement in a layered elastic crust’’ and ‘‘Stress in a stratified crust overlying a buried screw dislocation’’ by P.C. Leary. J. Geophys. Res., B 92, 4959–4964.

McGarr, A., 1988. On the state of lithospheric stress in the absence of applied tectonic forces. J. Geophys. Res., B 93, 13609–13617.

McGarr, A., 1991. On a possible connection between three major earthquakes in California and oil production. Bull. Seismol. Soc. Am. 81, 948–970.

McGarr, A., Gay, N.C., 1978. State of stress in the Earth’s crust. Annu. Rev. Earth Planet. Sci. 6, 405–436.

Mosher, D.C., Cassidy, J.F., Lowe, C., Mi, Y., Hyndman, R.D., Rogers, G.C., Fisher, M., 2000. Neotectonics in the Strait of Georgia: first tentative correlation of seismicity with shallow geological structure in southwestern British Columbia. Current Research 2000-A22. Geological Survey of Canada, pp. 1–9.

Olivieri, M., Ekstroem, G., 1999. Rupture depths and source processes of the 1997–98 earthquake sequence in central Italy. Bull. Seismol. Soc. Am. 89, 305–310.

Olson, J.A., Hill, P.H., 1993. Seismicity in the Southern Santa Cruz mountains during the 20-year period before the earthquake. In: Johnston, M.J.S. (Ed.), The Loma Prieta, California, Earthquake of October 17, 1989—Preseismic Observations. U.S. Geol. Surv. Prof. Paper, vol. 1550-C, pp. 3–16.

Oppenheimer, D.H., 1990. Aftershock slip behavior of the 1989 Loma Prieta, California earthquake. Geophys. Res. Lett. 17, 1199–1202.

Perfettini, H., Stein, R.S., Simpson, R.W., Cocco, M., 1999. Stress transfer by the 1988–1989 M = 5.3 and 5.4 Lake Elsman foreshocks to the Loma Prieta Fault; unclamping at the site of peak mainshock slip. J. Geophys. Res., B 104, 20169–20182.

Philip, H., Cisternas, A., Gvishiani, A., Gorshkov, A., 1989. The Caucasus: an actual example of the initial stages of continental collision. Tectonophysics 161, 1–21.

Philip, H., Rogozhin, E., Cisternas, A., Bousquet, J.C., Borisov, B., Karakhanian, A., 1992. The Armenian earthquake of 1988 December 7; faulting and folding, neotectonics and palaeoseismicity. Geophys. J. Int. 110, 141–158.

Reutter, K.J., Scheuber, E., Wigger, P. (Eds.), 1994. Tectonics of the Southern Central Andes. Springer Verlag, Heidelberg, p. 333.

Richins, W.D., Pechmann, J.C., Smith, R.B., Langer, C.J., Goter, S.K., Zollweg, J.E., King, J.J., 1987. The 1983 Bora Peak, Idaho, earthquake and its aftershocks. Bull. Seismol. Soc. Am. 77, 694–723.

Scandone, P., 1980. Origin of the Tyrrhenian Sea and Calabrian Arc. Boll. Soc. Geol. Ital. 98, 27–34.

Sibson, R.H., 1981. Controls on low-stress hydro-fracture dilatancy in thrust, wrench and normal fault terrains. Nature 289, 665–667.

Sibson, R.H., 1982. Fault zone models, heat flow, and the depth distribution of earthquakes in the continental crust of the United States. Bull. Seismol. Soc. Am. 72, 151–163.

Sibson, R.H., 1983. Continental fault structure and the shallow earthquake source. J. Geol. Soc. (Lond.) 140, 741–767.

Sibson, R.H., 1985. A note on fault reactivation. J. Struct. Geol. 7, 751–754.

Sibson, R.H., 1998. Brittle failure mode plots for compressional and extensional tectonic regimes. J. Struct. Geol. 20, 655–660.

Slejko, D., Neri, G., Orozova, I., Renner, G., Wyss, M., 1999. Stress Field in Friuli (NE Italy) from fault plane solutions of activity following the 1976 main shock. Bull. Seismol. Soc. Am. 89, 4.

Sparlin, M.A., Braile, L.W., Smith, R.B., 1982. Crustal structure of the eastern Snake River plain determined from ray trace modeling of seismic refraction data. J. Geophys. Res., B 87 (B4), 2619–2633.

Streit, J.E., Cox, S.F., 2001. Fluid pressure at hypocenters of moderate to large earthquakes. J. Geophys. Res., B 106, 2335–2343.

Townend, J., Zoback, M.D., 2000. How faulting keeps the crust strong. Geology 28, 399–402.

Triep, E.G., Aber, G.A., Lerner-Lam, A.L., Mishatkin, V., Zakharchenko, N., Starovoit, O., 1995. Active thrust front of the Greater Caucasus: the April 29, 1991, Racha earthquake se-

quence and its tectonic implications. J. Geophys. Res., B 100, 4011–4033.
Tsukahara, H., Ikeda, R., Omura, K., 1996. In-situ stress measurements in an earthquake focal area. Tectonophysics 262, 281–290.
Twiss, R.J., Moores, E.M., 1992. Structural Geology. Freeman, New York. 532 pp.
Vogfjörd, K.S., Langston, C.A., 1987. The Meckering earthquake of the 14 October 1968: a possible downward propagating rupture. Bull. Seismol. Soc. Am. 77, 1558–1578.
Wald, D.J., Heaton, T.H., Hudnut, K.W., 1996. The slip history of the 1994 Northridge, California, earthquake determined from strong motion, teleseismic, GPS and levelling data. Bull. Seismol. Soc. Am. 86, 549–570.
Wallace, R.E., 1984. Eyewitness account of surface faulting during the earthquake of 28 October 1983, Borah Peak, Idaho. Bull. Seismol. Soc. Am. 74, 1091–1094.
Weichert, D.H., Wetmiller, R.J., Munro, P., 1986. Vertical earthquake acceleration exceeding 2 g? The case of the missing peak. Bull. Seismol. Soc. Am. 76, 1473–1478.
Wetmiller, R.J., Horner, R.B., Hasegawa, H.S., North, R.G., Lamontagne, M., Weichert, D.H., Evans, S.G., 1988. An analysis of the 1985 Nahanni earthquakes. Bull. Seismol. Soc. Am. 78, 590–616.
Windley, B.F., 1995. The Evolving Continents. Wiley, Chichester. 526 pp.
Zelt, B.C., Ellis, R.M., Zelt, C.A., Hyndman, R.D., Lowe, C., Spence, G.D., Fisher, M.A., 2001. Three-dimensional crustal velocity structure beneath the Strait of Georgia, British Columbia. Geophys. J. Int. 144, 695–712.
Zoback, M.D., Townend, J., 2001. Implications of hydrostatic pore pressures and high crustal strength for the deformation of intraplate lithospere. Tectonophysics 336, 19–30.
Zollo, A., Marcucci, S., Milana, G., Capuano, P., 1999. The 1997 Umbria–Marche (Central Italy) earthquake sequence: insights on the mainshock ruptures from near source strong motion records. Geophys. Res. Lett. 26, 3165–3168.

Eugenio Carminati. PhD in 1997 with a thesis in Tectonophysics at the University of Milano. Post-doc from December 1996 to January 1998 at the Department of Geophysics of the University of Utrecht (the Netherlands). Post-doc from May 1998 to May 2000 at the Department of Earth Sciences of the University of Milano. Since September 2000 he works as University Researcher at the Department of Earth Sciences of the University of Roma 'La Sapienza'.

Carlo Doglioni. Since 1997 is a professor of geology at the University La Sapienza of Rome, Italy. He was formerly at the Universities of Basilicata, Bari and Ferrara. He visited as researcher the Universities of Basel, Oxford and Rice University of Houston. He works mainly geodynamics and field geology of the Mediterranean area. AAPG distinguished lecturer.

Salvatore Barba. PhD in 1999 with a thesis in Geophysics at the University of Roma 'La Sapienza'. Researcher at the Italian Seismic Survey in 1998. Since 1999 he is a Researcher at the Department of 'Seismology and Tectonophysics' of the Istituto Nazionale di Geofisica e Vulcanologia, in Roma.